Diel population dynamics and mortality of *Prochlorococcus* in the North Pacific Subtropical Gyre

Stephen J. Beckett[1,2,†,*], David Demory[1,2,‡,†,*], Ashley R. Coenen[2,3], John R. Casey[4,5,6,¶], Mathilde Dugenne[4,5,§], Christopher L. Follett[6], Paige Connell[7,8], Michael C.G. Carlson[9], Sarah K. Hu[7,10], Samuel T. Wilson[4,5,11], Daniel Muratore[1,2,12,13], Rogelio A. Rodriguez-Gonzalez[1,2,12], Shengyun Peng[1,2,14], Kevin W. Becker[10,15], Daniel R. Mende[4,5,16], E. Virginia Armbrust[17], David A. Caron[7], Debbie Lindell[9], Angelicque E. White[4,5], François Ribalet[17], and Joshua S. Weitz[1,2,3,18,*]

[1]School of Biological Sciences, Georgia Institute of Technology, Atlanta, GA, USA
[2]Center for Microbial Dynamics and Infection, Georgia Institute of Technology, Atlanta, GA, USA
[3]School of Physics, Georgia Institute of Technology, Atlanta, GA, USA
[4]Daniel K. Inouye Center for Microbial Oceanography: Research and Education, University of Hawai'i at Mānoa, Honolulu, HI, USA
[5]Department of Oceanography, University of Hawai'i at Mānoa, Honolulu, HI, USA
[6]Department of Earth, Atmospheric, and Planetary Sciences, Massachusetts Institute of Technology, Boston, MA, USA
[7]Department of Biological Sciences, University of Southern California, Los Angeles, CA, USA
[8]Biology Department, San Diego Mesa College, San Diego, CA, USA
[9]Faculty of Biology, Technion – Israel Institute of Technology, Haifa, Israel
[10]Department of Marine Chemistry and Geochemistry, Woods Hole Oceanographic Institution, Woods Hole, MA, USA
[11]School of Natural and Environmental Sciences, Newcastle University, Newcastle upon Tyne, UK
[12]Interdisciplinary Graduate Program in Quantitative Biosciences, Georgia Institute of Technology, Atlanta, GA, USA
[13]Santa Fe Institute, Santa Fe, NM, USA
[14]Adobe, San Jose, CA, USA
[15]GEOMAR Helmholtz Centre for Ocean Research, Kiel, Germany
[16]Laboratory of Applied Evolutionary Biology, Department of Medical Microbiology, Academic Medical Centre, University of Amsterdam, Amsterdam, The Netherlands
[17]School of Oceanography, University of Washington, Seattle, WA, USA
[18]Institut de Biologie, École Normale Supérieure, Paris, France

[‡]present address: Sorbone Université, CNRS, UMR 7232 Biologie Intégrative des Organismes Marins (BIOM), Observatoire Océanologique, Banyuls-sur-Mer, France
[¶]present address: Physical and Life Sciences Directorate, Lawrence Livermore National Laboratory, Livermore, CA, USA
[§]present address: Sorbonne Université, CNRS, UMR 7093, Laboratoire d'Océanographie de Villefranche-sur-Mer (LOV), Villefranche-sur-Mer, France

[†]These authors contributed equally.

[*]Corresponding authors: sjbeckett@gatech.edu, david.demory@obs-banyuls.fr, jsweitz@gatech.edu

Abstract

Light-driven forcing of cellular growth processes in the upper mixed layer of the ocean fuels primary and secondary production at the base of marine food webs. Motivated by high-frequency measurements taken by Lagrangian sampling in the North Pacific Subtropical Gyre (NPSG), we developed a hierarchical set of multi-trophic community ecology models to investigate and understand daily ecological dynamics in the near-surface ocean including impacts of light-driven growth, viral infection, and grazing on *Prochlorococcus*, the main primary producer in this ecosystem. Model-data fits reveal that integrating top-down processes with light-driven growth can jointly explain diel changes in cyanobacteria, (including infected cells), virus, and grazer abundances. Moreover, direct comparisons of *in silico* dynamics with *in situ* observations can be used to partition the relative contributions of viral-induced lysis and grazing to *Prochlorococcus* mortality. Model-based inferences estimate virus-induced lysis and grazing to contribute $< 5\%$ and $> 90\%$, respectively, to overall *Prochlorococcus* mortality – providing further support for recent observations that viral-induced lysis is relatively unimportant in shaping *Prochlorococcus* mortality in surface waters of the NPSG. While our results suggest grazing and viral-lysis explain $\approx 95\%$ of *Prochlorococcus* mortality, our model-data integration also finds that a modest, but nonetheless statistically significant component of estimated *Prochlorococcus* mortality ($\approx 5\%$ with 95% confidence intervals ranging from less than 1% to 27%) was not attributed to either viral lysis by T4- or T7-like cyanophages or grazing by heterotrophic nanoflagellates. Instead, model-data integration suggests the ecological relevance of other mortality mechanisms in structuring *Prochlorococcus* populations in the NPSG – likely by mixotrophic nanoflagellates, but potentially including grazing by other predators, lysis by other cyanophages, particle aggregation, and stress-induced loss mechanisms. Altogether, combining mechanistic multitrophic models with high-resolution measurements provides a route to quantify the balance of bottom-up and top-down forces in the NPSG while identifying the potential for non-canonical factors to shape the structure and function of marine microbial communities.

1 Introduction

Highly resolved surface ocean observations suggest that diel light rhythms drive repeatable changes in the abundance of ubiquitous picocyanobacteria at the base of the marine microbial food web, including both *Prochlorococcus* and *Synechococcus* [1, 2]. Phytoplankton population dynamics are influenced by both nutrient and light availability [2–11] as well as by density- and size-dependent feedback processes with other components of the community [12–18]. These interactions lead to diel oscillations in ecological rates, including in grazing rates, viral abundances, viral infection rates, and viral activity [19–24]. The emergence of diel rhythms in abundances and process rates raises the question: how does light-driven growth of photoautotrophs over day-night cycles influence oscillations of other microbial populations and ecosystem processes? Resolving this question is challenging because it is often hard to disentangle process from pattern, e.g., reduced population growth and/or increased mortality can have the same net effect on cyanobacterial abundances. This type of identifiability problem is inherent to prior efforts to model phytoplankton growth with a generic loss term, e.g. [2, 11–13]. The identifiability problem is compounded by the fact that daily rhythms of microbes are also entrained, in part, with oscillatory day-night light forcing. In this study, we set out to use an ecological modelling framework, combined with field observations that go beyond focusing just on cyanobacterial population measurements, as a means to understand how observed rhythms in *Prochlorococcus* dynamics influence and are influenced by rhythms of other populations in the microbial community in the North Pacific Subtropical Gyre (NPSG).

The NPSG is an oligotrophic system numerically dominated by the unicellular cyanobacterium *Prochlorococcus*, the most abundant phototroph in the global oceans [25]. Across oceanic basins, grazers and viruses are hypothesized to be the dominant drivers of *Prochlorococcus* loss [26, 27]. However, estimating the relative contribution of viral-induced mortality and grazing-induced loss at a particular site remains challenging [23, 28–31]. We focus our analysis on a near-surface Lagrangian parcel of water in the NPSG, which was sampled at high resolution in the upper mixed layer at 15m depth over the course of ten days in summer 2015 in the SCOPE HOE-Legacy 2A cruise (see Methods for more details). Prior work from this cruise using the cellular iPolony method estimates that viruses, despite being highly abundant, contribute to less than 5% of total *Prochlorococcus* cellular losses per day [23]. In parallel, analysis of food requirements to maintain heterotrophic nanoflagellates abundances on this cruise suggest that grazing could account for the majority of *Prochlorococcus* cell losses per day [24]. However, this quota method cannot rule out the potential for significantly lower rates of grazing, especially if *Prochlorococcus* represent only a part of the diet of heterotrophic nanoflagellates. Resolving the partitioning of cyanobacterial mortality amongst different pathways is important for understanding both microbial ecology and ecosystem

functioning. The loss of microbes due to grazing is expected to drive the flow of matter upwards through marine food webs and out of the surface ocean ecosystem by way of export via fecal pellet production and subsequent sinking [32]. In contrast, viral infection and lysis is expected to shunt matter back into the microbial loop [33–35], though significant lysis (e.g., during bloom events) may lead to production of sticky aggregates that increase export out of the surface ocean [36, 37].

Here, we synthesized and integrated data from the 2015 cruise; augmented by the development, fitting, and comparison with multi-trophic community ecology models. Our primary aim was to understand how mechanistic interactions between cyanobacteria, viruses, and grazers could explain the observed diel variation in population abundances, process rates, and aggregate community dynamics in a model ocean ecosystem. To do so, we developed nonlinear population dynamic models of microbial interactions spanning the cyanobacterium *Prochlorococcus*, heterotrophic nanoflagellate grazers and T4- and T7-like cyanophages in an oscillating light environment. These models combine principles of microbial interactions, including virus-microbe interactions [31, 38–43], with light-driven forcing of cellular physiology [2, 12]. We use these models to examine a series of related questions: how is the community expected to behave over diel timescales and how does light-driven forcing of cyanobacterial growth affect interactions between marine prey and predators? To do so, we compare *in silico* and *in situ* ecological rhythms as a means to identify whether mechanistic representations of feedback can recapitulate observed timeseries and, if so, to what extent we can disentangle the relative contribution of viral-induced lysis and grazing to total *Prochlorococcus* mortality. As we show, model-data integration suggests that the tight coupling of *Prochlorococcus* growth and loss over diel cycles may not be controlled only by cyanophages and heterotrophic grazers, but that additional loss factors may also be ecologically relevant, raising new questions on governing mechanisms at the base of the marine food web.

2 Modelling Framework

2.1 Overview of Model Structure

We developed a mechanistic mathematical model of an Ecological Community driven by Light including Infection of Phytoplankton (ECLIP). Our model includes dynamics of *Prochlorococcus*, grazers, and viruses, as well as *Prochlorococcus* division and loss, where the loss arises due to a combination of grazing, viral lysis, and other factors (see Figure 1a for a schematic overview). In this model, viruses correspond to the abundances of types T4- and T7-like cyanophages which are known to primarily infect *Prochlorococcus*. The grazers represent heterotrophic nanoflagellates which can feed on multiple prey types [44], however the primary food source for heterotrophic nanoflagellates could be *Prochlorococcus* [24]. As a result, we introduced flexibility in our model framework to account for the extent to which *Prochlorococcus* constitutes the primary source of food for the observed grazer class. To assess this uncertainty we investigated models of six grazer strategies, ranging from a "specialized" grazer class that exclusively consumes *Prochlorococcus* cells ($\gamma = 0$ day^{-1}) to models with increasing levels of generalism ($\gamma = 0.01$ to $\gamma = 0.5$ day^{-1}) representative of grazers that consume additional prey sources, e.g., heterotrophic bacteria which are not explicitly integrated into the multitrophic model. Mixotrophic nanoflagellates [45] were observed at the study site, but are thought to contribute less to the grazing pressure on the bacterial community compared to heterotrophic nanoflagellates [24]. As it was not possible to differentiate abundance measurements of mixotrophic nanoflagellates from phototrophic nanoflagellates [24], we focus our attention on grazing by heterotrophic nanoflagellates. Across the gradient of specialism-generalism grazer models, we searched for sets of ecological parameters that are biologically feasible and used a model-data integration approach to identify parameter sets that generate dynamics consistent with the observed population dynamics in the NPSG. A complete description of the model structure and justifications for functional and parameter choices are found in the Supplementary Methods.

2.2 Ecological model of phytoplankton communities with viral and grazer mediated predation (ECLIP)

The ECLIP model represents *Prochlorococcus* cell division as a light-driven process (where cell division is expected to occur at night [2, 46]) and *Prochlorococcus* cell losses are controlled by viral lysis, grazing, and other density-dependent factors (Figure 1). The *Prochlorococcus* population is structured by two states of infection: cells that are susceptible to viral infection (S) and cells that are infected (I) by viruses (V). Grazers (G) feed indiscriminately on both S and I classes. The dynamics of the abundances of S, I, V

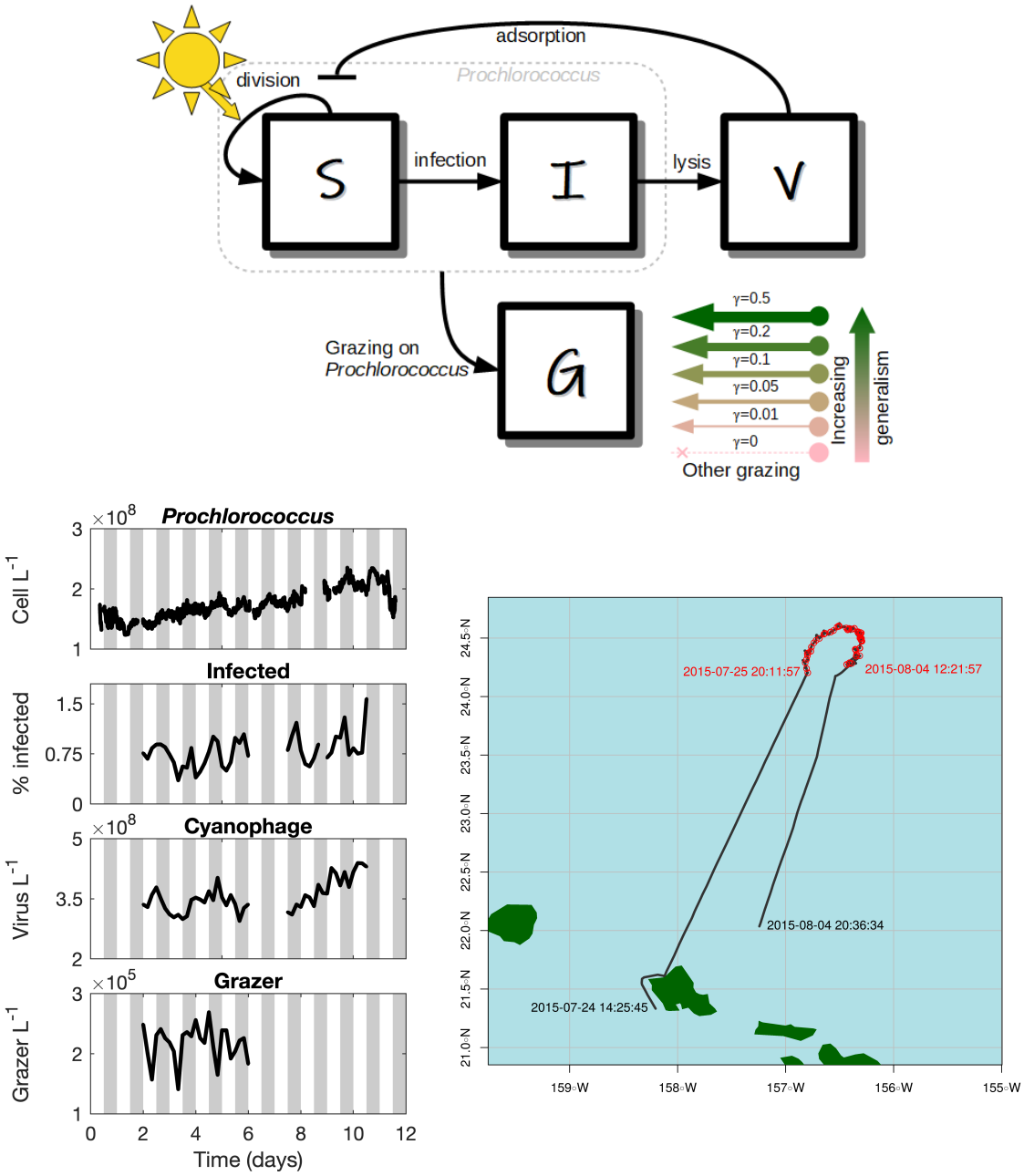

Figure 1: Community ecological model of viral and grazer mediated predation; and field data from the SCOPE HOE-Legacy 2A cruise. *Prochlorococcus* are structured by viral infection status. Virus particles (V) can infect susceptible *Prochlorococcus* cells (S) generating infected cells (I). Viral-induced lysis of infected cells releases virus particles back into the environment. Both susceptible and infected *Prochlorococcus* cells are subject to grazing pressure from heterotrophic nanoflagellate grazers (G). Additionally, grazers may have a generalist strategy (e.g., grazing on heterotrophs, mixotrophs and phytoplankton not represented by S and I). We specify six models along this specialism-generalism gradient by setting a parameter γ. When $\gamma = 0$ heterotrophic nanoflagellate grazers act as specialists and only consume *Prochlorococcus*; and as the value of γ increases, *Prochlorococcus* constitutes less of the diet of heterotrophic nanoflagellate grazers. Full specification of parameters and units is found in Table S1. (b) Empirically measured population dynamics of *Prochlorococcus* cells, the percentage of *Prochlorococcus* cells infected with T4/T7-like cyanophage, the abundance of free-living T4/T7-like cyanophage, and the abundance of heterotrophic nanoflagellate grazers. Grey bars indicate nighttime. (c) Map of cruise track and sampling stations. Local times (HST) for the start and end of recorded underway sampling (shown as the black line), and the first and last sampling stations (shown as red points) are annotated.

and G over time are described by the following system of equations:

$$
\begin{aligned}
\frac{dS}{dt} &= \overbrace{\mu(t)S}^{division} - \overbrace{m_P S(S+I)}^{higher\text{-}order\ losses} - \overbrace{\phi SV}^{infection} - \overbrace{\psi SG}^{grazing} \\
\frac{dI}{dt} &= \overbrace{\phi SV}^{infected} - \overbrace{m_P I(S+I)}^{higher\text{-}order\ losses} - \overbrace{\eta I}^{viral\text{-}lysis} - \overbrace{\psi IG}^{grazing} \\
\frac{dV}{dt} &= \overbrace{\beta\eta I}^{viral\ production} - \overbrace{\phi(S+I)V}^{adsorption} - \overbrace{m_V V^2}^{higher\text{-}order\ losses} \\
\frac{dG}{dt} &= \overbrace{\epsilon\frac{N_P}{N_G}\psi(S+I)G}^{grazing\ on\ Prochlorococcus} + \overbrace{\gamma G}^{generalist\ grazing} - \overbrace{m_G G^2}^{higher\text{-}order\ losses} ,
\end{aligned}
\tag{1}
$$

where

$$
\mu(t) = \mu_{ave}\,(\ 1\ +\ \delta_\mu \sin(\ 2\pi(t+\delta_t)\ )\ ) . \tag{2}
$$

Prochlorococcus have a diel-driven population division rate $\mu(t)$ whose proportional amplitude and phase are set by parameters δ_μ and δ_t respectively, and $t = 0$ represents 06:00:00 local time (where t is measured in days) (see Figure S1 for a visualization of the diel-driven division rate). *Prochlorococcus* have a nonlinear loss rate, m_P, dependent on total phytoplankton abundance, to implicitly represent niche competition [47]. Viruses infect susceptible *Prochlorococcus* at a rate ϕ. For each infection a burst size β of new virions are released into the environment upon cellular lysis following the latent period (with average duration $\frac{1}{\eta}$). Grazing upon *Prochlorococcus* is non-preferential with respect to infection status and occurs at a rate ψ. Consumption of *Prochlorococcus* biomass is converted into grazer biomass with Gross Growth Efficiency (GGE) ϵ and is assumed proportional to a nitrogen currency, given the nitrogen content in a *Prochlorococcus* cell (N_P) and a grazer (N_G), leading to an effective GGE of $\epsilon\frac{N_P}{N_G}$. We introduce γ as a parameter to denote the level of generalism in grazing, where the term represents net additional gains to the grazer from non-*Prochlorococcus* prey sources after accounting for respiratory costs. We represent a specialist strategy via $\gamma = 0$ day^{-1}, assuming that *Prochlorococcus* cells are the only source of grazer sustenance. In contrast, we represent five generalist strategies via $\gamma = 0.01$ (very low), 0.05 (low), 0.1 (medium), 0.2 (high), or 0.5 (very high) day $^{-1}$, implying that grazers have a net positive growth rate even in the absence of S or I via the consumption of other phytoplankton, heterotrophic bacteria, or grazers (via intraguild predation). We note the exact degree to which grazers act generalists, rather than specialists on *Prochlorococcus*, is dependent on other life-history traits (equation S20) and so is not set explicitly in our model. Grazer and viral losses from the system are both characterized by nonlinear loss terms (respectively with rates m_G and m_V) to avoid structurally biasing the model to favour one of these types of *Prochlorococcus* predators [31] and to avoid competitive exclusion between grazers and viruses. Linear loss terms were excluded in order to reduce the number of free parameters to estimate via inference. A full list of parameters and further details are shown in the Supplementary Information (see Table S1 for parameter definitions and Table S2 for specification of parameter priors).

2.3 *in situ* measurements

We use data collected from the SCOPE HOE-Legacy 2A cruise in Summer 2015. Measurements of total *Prochlorococcus* abundance were made every ≈3 minutes, with measurements of infected cells (infected by either T4- or T7-like cyanophages), total virus particles of either T4- or T7-like cyanophages, and heterotrophic nanoflagellate grazers collected at 4 hr intervals over a multi-day period aboard the R/V Kilo Moana. In all figures, the 12 days shown represent the time between 06:00:00 24th July 2015 and 06:00:00 August 5th 2015 local time. The following summarizes the collection methods for each *in situ* time series analyzed in this paper.

***Prochlorococcus* cell abundance:** The SeaFlow, a shipboard *in situ* flow cytometer, continuously measures forward scattering, red and orange fluorescence intensities of particles ranging in size from ~0.4 to 4 μm in diameter from underway samples (continuously pumped surface sea water from ~7 m depth) every 3 minutes. A combination of manual gating and statistical methods was used to identify *Prochlorococcus* based on forward scatter (457/50 bandpass filter), orange fluorescence (572/28 bandpass filter) and red fluorescence (692/40 band-pass filter) relative to 1-μm calibration beads (Invitrogen F8823). Cell diameter of individual cells was estimated from SeaFlow-based light

scatter by the application of Mie light scatter theory to a simplified optical model, using an index of refraction of 1.38 [48–50]. Data was obtained via Simons CMAP [51].

Virus abundance and infection: Samples for virus abundance and infection were collected every 4 hours at 15 m depth using a CTD-rosette equipped with 12 L niskin bottles [23]. Samples for cyanophage abundances (40 mL) were filtered through a 0.2 μm syringe top filter, flash frozen, and stored at -80°C. Samples for infected cells (40 mL) were filtered through a 20 μm nylon mesh, fixed with electron microscopy grade glutaraldehyde (0.125% final concentration), incubated for 30 minutes in the dark at 4°C, flash frozen, and stored at -80°C. Cyanophage concentrations were analyzed using the polony method for T7-like [52] or T4-like [53] cyanophage families. Virally infected *Prochlorococcus* was quantified using the iPolony method [23] in which *Prochlorococcus* cells were sorted with a BD Influx cytometer and screened for intracellular T4-like and T7-like cyanophage DNA.

Measurements of heterotrophic nanoflagellates: Samples for nanoplankton (protists 2-20 μm in diameter) abundances were collected every 4 hours at 15 m depth [24]. Subsamples were preserved with formaldehyde (final concentration 1%, final volume 100 mL) and were stored at 4°C. Slides were prepared from preserved samples within 12 hours of sampling by filtering 100 mL subsamples down to ~1 mL onto blackened 2 μm, 25 mm polycarbonate filters and staining the samples with 50 μL of a 4'-6'diamidino-2-pheylindole (DAPI, Sigma-Aldrich, St. Louis, MO) working solution (1 mg mL^{-1}) for 5-10 minutes in the dark [54]. Stained samples were filtered and rinsed; filters were placed on glass slides with a drop of immersion oil and coverslip, then sealed with clear nail polish. Slides were stored at -20°C until analysis. Heterotrophic nanoplankton abundances were counted using epifluorescence microscopy from triplicate slides, and differentiated from photo/mixotrophic nanoplankton by the lack of chlorophyll *a* autofluorescence in plastidic structures when viewed under blue-light excitation [24].

2.4 Model-data integration

In order to constrain the ECLIP models to data, we determined the life-history parameter sets for the ECLIP model that optimized the fitting of model dynamics to field measurements using Markov Chain Monte Carlo (MCMC), as implemented in the probabilistic inference package Turing [55] in the Julia language [56]. MCMC is a class of Bayesian inference algorithms that aims to infer the probability distribution of model parameters given the structure of model equations, data, and prior parameter distributions [57]. We used the No-U-Turn Sampler (NUTS) implemented in Turing to sample the posterior distributions [58] (our choices of prior distributions are described in Table S2). Classic Hamiltonian Monte Carlo (HMC) algorithms are sensitive to the number of steps of the simulation reducing the performance of the algorithm in high-dimension problems. NUTS is an alternative algorithm for MCMC that eliminates the need to set the number of steps, allowing better performance for high-dimensional parameter space and non-linear dynamic models [58]. Further details are described in the Supplementary Information.

2.5 Model availability

Code for ECLIP and performing Bayesian parameter inference was written and run in Julia, with plotting performed in MATLAB. Core code for running model simulations, analysis and plotting is archived on Zenodo [59].

3 Results

3.1 Fitting the ECLIP model to field measurements of *Prochlorococcus*, cyanophages, and grazers

Time series data from the 2015 SCOPE HOE-Legacy 2A cruise reveals that *Prochlorococcus* cell abundances are periodic, peaking at night [23]. Population abundances of heterotrophic nanoflagellates fluctuate with unclear periodicity [24], as do the abundances of T4- and T7-like cyanophage [23]. In contrast, the fraction of cells infected by of T4- and T7-like viruses [23] are periodic, peaking during the night. For all patterns, see Figure 1b. The periodicity of infected cells suggests the potential for emergent synchronization of processes in the food web driven by diel-driven dynamics, similar to emergent synchronization

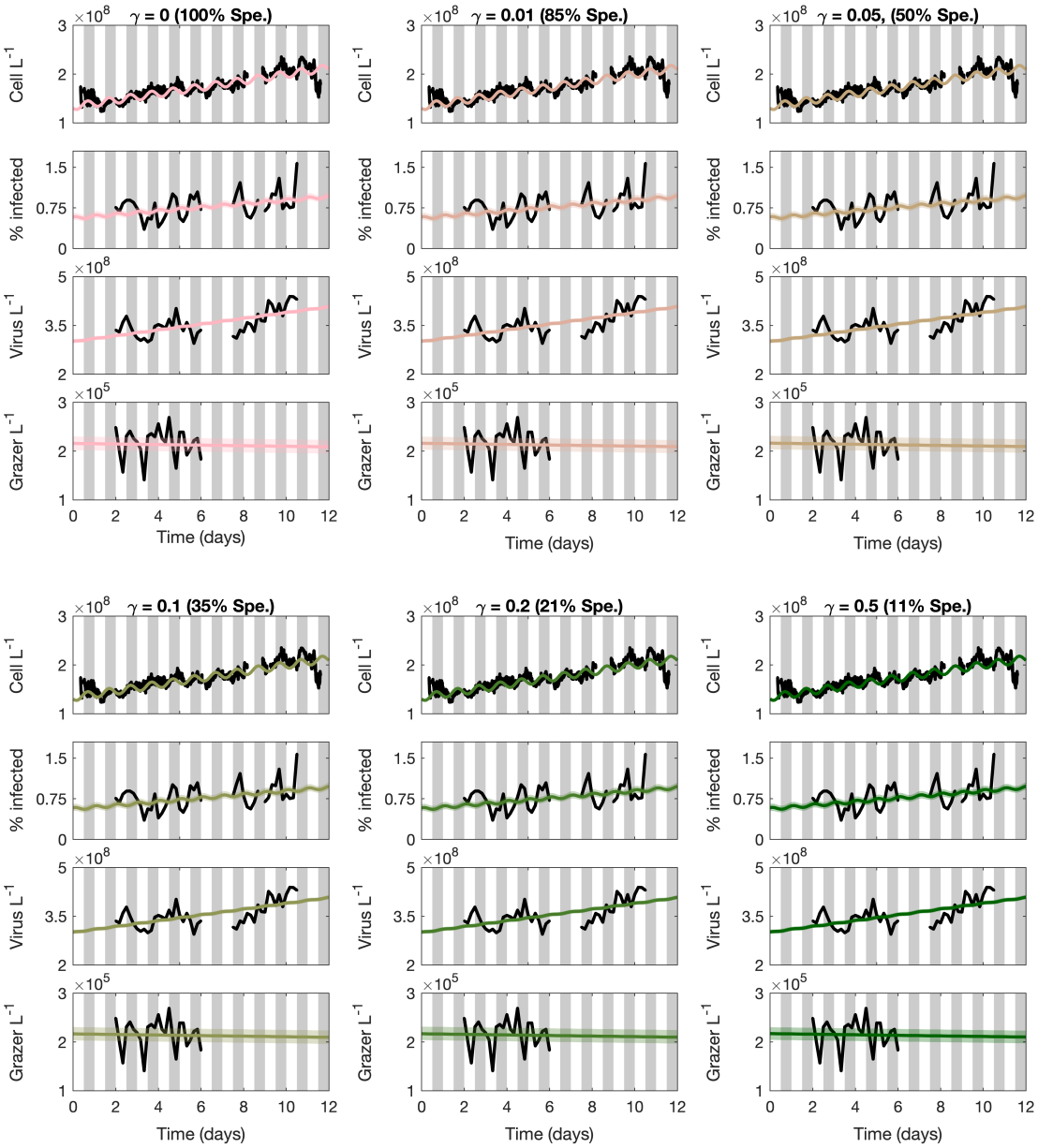

Figure 2: Models across the specialism-generalism gradient fit empirical data. ECLIP models are compared against empirical data in black. Model lines represent the median MCMC solution within 95% CI range found by the converged chains, shown as bands with colours representing the choice of γ. Data signals include *Prochlorococcus* cell abundances (top), the percentage of infected *Prochlorococcus* cells, the abundance of free viruses and the abundance of heterotrophic nanoflagellate grazers (bottom). The models were fitted against detrended data; for visualization we have added these trends to the model solutions. Grey bars indicate nighttime. Model solutions with: (a) $\gamma = 0$ (grazers act as specialists), (b) $\gamma = 0.01$, (c) $\gamma = 0.05$, (d) $\gamma = 0.1$, (e) $\gamma = 0.2$, (f) $\gamma = 0.5$ day^{-1}. The degree of grazer specialism (Spe.) is shown in parentheses above each subplot.

in community-wide metabolism in the NPSG [60]. Here, we synthesized and integrated these datasets in the context of the ECLIP model (see Methods).

To explore potential coexistence dynamics of *Prochlorococcus*, viruses and grazers, we fit the ECLIP model using a Bayesian inference approach given parameter bounds in biologically realistic ranges (see Table S1 for prior parameters, Figure S2 for division-associated priors, and the Supplementary Information S2 for information on the MCMC fitting procedure). The models are fitted against detrended empirical data, so for visualization we add this trend to the model simulations. The ECLIP models,

with differing levels of grazer generalism parameter γ, fitted to the observations are shown in Figure 2. All ECLIP models were able to simultaneously reproduce the magnitudes of the different timeseries and produced fits with similar log-likelihoods (see Figure S9) while exhibiting statistical evidence of convergence (see Figure S5 and Figure S8). Hence, based on fitting data alone it is not feasible to identify a particular, preferred level along the specialist-generalist grazer gradient. In sum, we find that a range of nonlinear mathematical model including feedback between cyanobactaeria, cyanophage, and grazers can jointly recapitulate multi-trophic population dynamics in the NPSG. However, despite fitting overall magnitudes and oscillations in *Prochlorococcus* abundances, the ECLIP model underestimated the strength of oscillations in infected cells (an issue we return to in the Discussion).

3.2 Interpretation of ecological mechanisms underlying model-data fits

The equivalence in model-data fit convergence across a spectrum of grazer generalism suggests that differentiating model mechanisms requires inspection and interpretation of posterior parameter fits. In Figure 3 we show that the choice of γ corresponds to representing a grazer specialism-generalism gradient in the inferred ECLIP models, with relative *Prochlorococcus* consumption decreasing with increasing generalism γ, as expected (but note, this was not a guaranteed result due to the dependence of the degree of generalism on other life-history traits (equation S20)). However, absolute per capita consumption of *Prochlorococcus* only varied modestly (≈0.04-0.075 per day) between models. Hence, the per-capita mortality of *Prochlorococcus* due to grazing remains relatively invariant to model choice, even as grazer uptake of other organisms increases with increasing γ. We interpret this finding to suggest that disentangling the level of grazer generalism requires direct investigation of uptake rates of other food sources (e.g., hetetrophic bacteria) for nanoflagellate grazers in the NPSG.

The full set of posterior parameter values along the grazer generalism gradient are shown in Figure 4, with full details on the fits of the division function in Figure S3 along with comparison of priors and posterior parameter values in Figure S4. Most life-history traits converge to similar values in parameter space across ECLIP models, with a notable exception: there is a systematic trend in the grazer loss parameter m_G, reflecting a trade-off between grazer losses and grazer gains via increasing γ. We find that the inferred grazer loss rates correspond to grazer residence times of between 16.81 (95% CI: 15.37-20.19) days in the specialist model to 1.82 (95% CI: 1.8-1.87) days in the most generalist model when $=$ 0.5 per day. This range is consistent with estimated heterotrophic nanoflagellate doubling times in the Mediterranean Sea [61]. The corresponding virus residence times were estimated as 1.16 days (95% CI: 0.59-5.3 days) in the specialist model and 1.17 days (95% CI: 0.57-8.32 days) when $= 0.5$ (see Figure S10). MCMC parameter distributions appear tight (e.g. for μ_{ave}, δ_t, and ϕ) or loose (e.g. for β, m_P and m_V) suggesting different parameter sensitivities in the parameter space [62]. We interpret the relative loose sensitivity of model output to mean that examination of residence times of grazers and viruses in the NPSG could help differentiate model classes.

3.3 Partitioning the daily losses of *Prochlorococcus* between top-down and other effects

We analyzed the predicted partitioning of *Prochlorococcus* mortality among grazing by heterotrophic nanoflagellates, viral-induced lysis by T4- and T7-like cyanophages, and other sources of mortality, using the inferred ECLIP models. In each case, we used posterior parameter estimates from model-data fits as a means to estimate total *Prochlorococcus* loss rates:

$$m_{total} = m_{\text{lysis}} + m_{\text{grazing}} + m_{\text{other}} \tag{3}$$

where: $m_{\text{lysis}} = \eta I$, $m_{\text{grazing}} = \psi(S+I)G$, $m_{\text{other}} = m_P(S+I)^2$ (see the Supplementary Information for more details). The proportion of each mortality process is then calculated as the average ratio of the component mortality rate relative to that of the total over the empirical time-series. Mortality partitioning derived from model-data fits suggest that 87-89% (with extents of 95% confidence intervals ranging from 66% to 96%) of *Prochlorcoccus* losses were ascribed to grazing, 6% (with extents of 95% confidence intervals ranging from 4% to 9%) to viral lysis and 4.5-6.6% (with extents of 95% confidence intervals ranging from less than 1% to 27%) to other mechanisms. The distribution of losses by category are shown in the top six rows of each panel in Figure 5. The top six rows denote distinct levels of grazer generalism, from $\gamma = 0$ to $\gamma = 0.5$. Notably, inferred mortality estimates from fitting ECLIP models to field data were comparable regardless of the level of grazer generalism. Hence, the emergent feature of mortality partitioning is robust to model choice. This robustness also suggests that other functional

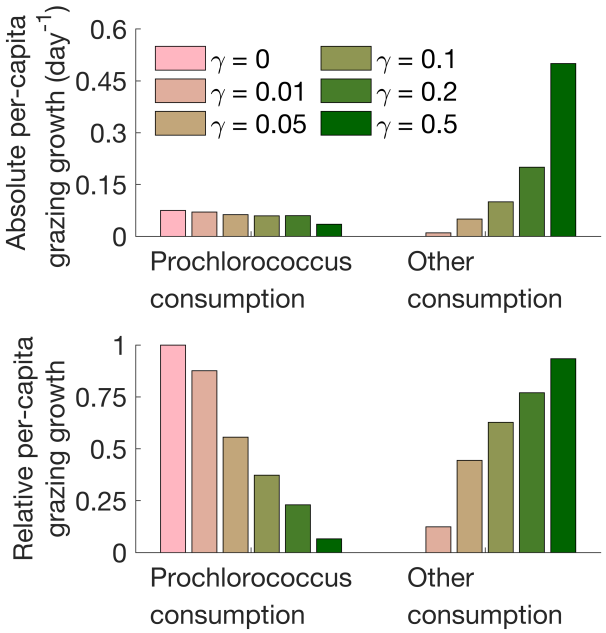

Figure 3: Model differences across the specialist-generalist gradient. (a-b) Inferred grazer growth attributable to consumption of *Prochlorococcus* or other sources (see equation S20) across models.

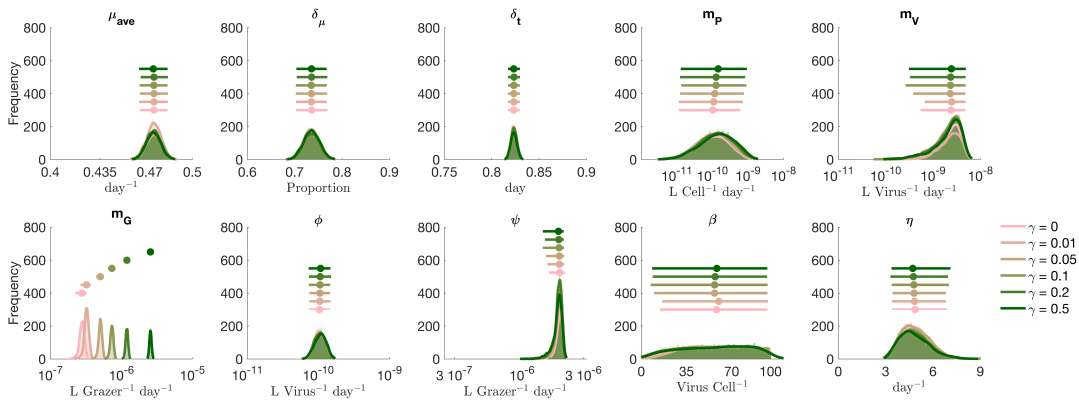

Figure 4: Differences in inferred life-history traits across the specialist-generalist gradient. (a-j) Parameter posterior distributions for different ECLIP models. Parameters are (a) μ_{ave}: average *Prochlorococcus* division rate, (b) δ_μ: division rate amplitude, (c) δ_t: phase of division rate, (d) m_P: higher order *Prochlorococcus* loss rate, (e) m_G: higher order viral loss rate, (f) m_G: higher order grazer loss rate, (g) ϕ: viral adsorption rate, (h) ψ: grazer clearance rate, (i) β: viral burst size, and (j) η: viral-induced lysis rate. Jittered median (dot) and 95% CI range (horizontal line) for each of the models are shown above density plots. Full details of parameter bounds are shown in Table S1; see Supplementary Information for more details.

processes or ecosystem indicators may be decisive in disentangling the extent of grazer generalism in the system. The other take-away from this analysis is that grazer induced losses predominate when jointly estimating the collective effects of grazers and viruses on multi-trophic population dynamics. Yet, notably, other forms of losses may be as ecologically relevant as viral induced mortality to daily *Prochlorococcus* losses.

3.4 Contrasting model-derived to empirical estimates of *Prochlorococcus* losses

Model-data integration using ECLIP leverages multitrophic signals to simultaneously infer the putative daily loss of *Prochlorococcus* in the upper mixed layer due to grazing, viral lysis and other loss mech-

anisms. These joint estimates can be compared to alernative methods that estimate loss rates due to viral infection or grazing, albeit one factor at a time. There are multiple existing approaches to infer *Prochlorococcus* loss rates *in situ*. In the case of viral lysis, we consider two methods: (i) encounter theory; (ii) iPolony estimates. Conventional 'encounter' based estimators for viral lysis use biophysical theory to estimate an upper-limit of size-dependent contact rates. However, encounter need not imply a successful adsorption and lysis event, hence the realized level of lysis via encounter theory can often be significantly less than that expected from biophysical limits [17]. In contrast, the iPolony method quantifies the fraction of host cells infected by a target phage, which can be combined with estimates of viral latent periods and cell division rates to infer daily loss rates [23] (see Supplementary Information for more details). In the case of grazing, we consider three methods: (i) encounter theory; (ii) quota-based theory; (iii) flourescently-labeled bacteria (FLB) estimates. For grazers, size-dependent encounter rate theory and quota-based theories use biophysical contact rates and allometrically derived carbon and elemental growth requirements, respectively, to estimate grazing induced loss rates. Theoretical estimates via the encounter and quota methods have significant variability due in part to uncertainties in life-history traits. FLB is a direct method, insofar as it uses quantification of uptake of a surrogate prey (*Dokdonia donghaensis* – see details in Connell et al. [24]) of a similar size to target cyanobacteria as a proxy for uptake rates.

Figure 5 compares *joint* ECLIP-inferred estimates of relative mortality (reported in the prior Section) with *one-factor* estimates from field-based (iPolony measurements and fluorescently labelled bacterial (FLB) uptake estimates) and alternative, theoretical methods (both encounter and quota). See Supplementary Information S1 for extended details. In the case of viral lysis, one-factor estimates using encounter theory do not constrain daily loss rates, given that contact-limited lysis rates are compatible with nearly 100% of observed *Prochlorococcus* loss; but decreases in contact, efficiency of adsorption, and inefficiency of infection post-lysis lead to poorly constrained lower limits (see Supplementary Information for more details). In contrast, direct estimates of infection processes in the NPSG via the iPolony method over the diel cycle suggest that viral-induced lysis by T4- and T7-like cyanophages contribute a comparatively small amount to *Prochlorococcus* cell losses (consistently less than 5% throughout the observed period). Likewise, accounting for observed grazer abundances and biophysically plausible grazing rates suggests that grazing could potentially explain daily *Prochlorococcus* losses alone. But, the lower limits of theory based estimates of grazing induced mortality - as was the case for viral-induced mortality - are poorly constrained given uncertainties in grazing efficiency. Notably, empirically-derived estimates using the FLB method suggest that grazing by heterotrophic nanoflagellates accounts for $\approx 30\%$ of total *Prochlorococcus* loss rates – though we note the original experiment was designed to differentiate relative grazing by mixotrophic and heterotrophic nanoflagellates. If both the iPolony and FLB methods were unbiased, then the majority of loss rates would be unaccounted for by top-down effects.

Instead, our comparison of ECLIP-inferred and one-factor estimates provides evidence to constrain the influence of top-down vs. bottom-up factors. Like the iPolony method, all of our joint ECLIP-inferred estimates across a spectrum of grazer generalist assumptions are consistent with the conclusion that viral-induced lysis is responsible for a small proportion of cellular losses. We note that ECLIP-inferred viral lysis estimates are approximately 3% higher than those inferred from iPolony (an issue we return to in the Discussion). In contrast, joint ECLIP-inferred estimates suggest that grazing by heterotrophic nanoflagellates represent the majority of *Prochlorococcus* cell losses across the ECLIP models – far above that inferred via FLB experiments. Notably, we found that estimates of *Prochlorococcus* losses via grazing were robust to changes in grazer specialism, further suggesting that FLB-derived estimates may under-represent the extent of *in situ* grazing (which could represent biological or methodological uncertainty [24]). Additionally, we found that the model-inferred combination of viral-induced lysis by T4- and T7-like cyanophages and grazing by heterotrophic nanoflagellates typically do not sum up to equal total *Prochlorococcus* cell losses on a daily basis. Instead, our model-data integration suggests that other sources of *Prochlorococcus* cell losses account for $\approx 5\%$ of daily losses (with 95% confidence intervals ranging from less than 1% to 27%). Together, both model-data fits and independent estimates of top-down mortality suggest that other forms of losses beyond grazing by heterotrophic nanoflagellates and lysis by T4/T7-like cyanophages may be critical in shaping daily phytoplankton rhythms.

4 Discussion

We developed and analyzed a multitrophic community ecology model consisting of *Prochlorococcus*, viruses, and grazers to investigate the feedback mechanisms and ecological drivers of oligotrophic ocean microbial population dynamics on diel timescales. The ECLIP model includes light-driven phytoplank-

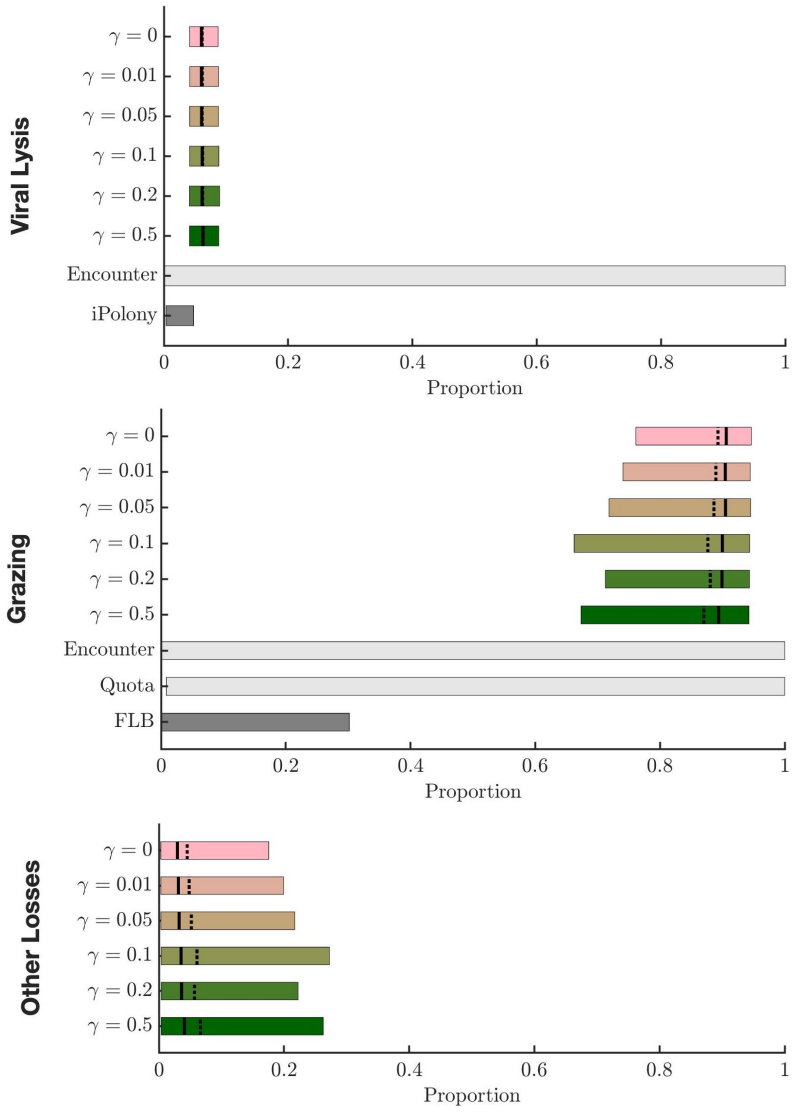

Figure 5: Relative importance of viral lysis, grazing, and other effects on total *Prochlorococcus* mortality. The proportion of mortality partitioned between viral-induced lysis (top panel), grazing (middle panel), and other (bottom panel) sources for the ECLIP models and other measures of relative mortality. For ECLIP the results from all chains are shown. Bars in these panels denote mortality rate proportions associated with the 95% confidence intervals, where the mean and median are shown by solid and dashed lines, respectively. Other measures of relative mortality are given via theoretical encounter rates and quota based estimates, direct measurements of viral infection (iPolony), and Fluorescently Labelled Bacteria (FLB) incubation measurements (see Supplementary Information Section S1 for details).

ton growth, where phytoplankton can be infected and lysed by viruses, or grazed upon by heterotrophic nanoflagellate grazers. We found that ECLIP is capable of recapitulating the dynamical coexistence of populations of cyanobacteria, viruses infecting cyanobacteria, and grazers, and that the suite of model solutions encompasses the population abundances observed in the NPSG. By combining model-data fits with direct measurements of mechanistic interactions we infer that grazing is the predominant loss factor for *Prochlorococcus* and that viral lysis is a relatively unimportant factor in shaping *Prochlorococcus* mortality on diel time scales in surface waters of the NPSG. We also find that the combination of lysis and grazing does not fully account for daily *Prochlorococcus* losses. Instead, model inference suggests that a non-trivial amount of *Prochlorococcus* losses are due to other mechanisms beyond that of top-down lysis by T4- and T7-like cyanophage and heterotrophic nanoflagellate grazing.

Our development of a multitrophic model focused in on a portion of a complex surface ecosystem. In doing so, we integrated our nonlinear population dynamic models with field observations to understand interactions of T4- and T7-like cyanophages as well as heterotrophic nanoflagellate grazers with

Prochlorococcus, the most abundant phytoplankton at our study site. Prior work, e.g. [24], has assumed that *Prochlorococcus* is the predominant prey for heterotrophic nanoflagellate grazers - but such an assumption had the potential to bias interpretations of direct ingestion experiments (and the interpretation of total loss rates). Instead, it is likely that heterotrophic nanoflagellate grazers rely on other food sources as part of a generalist feeding strategy. Indeed, there may be a suite of specialist to generalist grazing strategies embedded within the community of heterotrophic nanoflagellates which in turn may depend on physiological status and/or environmental cues [63, 64]. To evaluate this unknown variation, the ECLIP framework included the potential for model outcomes to span generalist to specialist grazing strategies. However, we found a critical identifiability problem: a broad range of model classes could explain population dynamics. These identifiability problems within the ECLIP framework prevent us from distinguishing whether heterotrophic nanoflagellates act primarily as specialist grazers of *Prochlorococcus*, or ingest a broader range of prey items. We also inferred that some life-history traits covaried within the suite of ECLIP models (see Figures S6-S7). In particular, we found strong parameter correlations between adsorption rates and latent period, burst size and the viral loss rate, as well as between clearance rates and grazer and *Prochlorococcus* loss rates (Figure S7). Covariation of parameters indicates that further measurements are likely required to disentangle models that fit diel time series data, albeit with different underlying quantitative mechanisms.

Box 1 | Potential mechanisms to explain other losses of *Prochlorococcus*

Undercharacterized ecological interactions

Mixotrophic nanoflagellates do contribute to grazing upon *Prochlorococcus*, with measurements suggesting this is a smaller contribution relative to the heterotrophic nanoflagellates [24, 65] – but still likely significant [66, 67]. Evaluating *in situ* mixotrophy is an ongoing challenge. Additionally, unknown viruses that are not quantified by the iPolony method (e.g. cyanophage without an identifiable DNA polymerase gene [68], or perhaps RNA viruses), as well as other grazer types including larger consumers may be contributing to the 'other mortality' terms in our models. In addition, the model includes viral-induced and grazing-induced losses; however in both cases we utilise a contact-driven model, analogous to 'Type I' functional responses. Mechanistic changes in functional responses and/or responses to light may drive distinct interaction rates (and aggregate mortality) even given the same set of viruses and grazers.

Aggregation and sinking of picoplankton

Some losses may be due to *Prochlorococcus* aggregation, particle attachment, and subsequent sinking out of the mixed layer. Picoplankton (and their viruses) have been suggested to be an important contributor to export in large scale analyses e.g. [69, 70], though Guidi et al. [70] suggest *Synechococcus* rather than *Prochlorococcus* abundances appear correlated to export. Additionally, less is known about the microscale processes that might lead to export contributions from picoplankton – *Prochlorococcus* cells can be grown and sustained in laboratory culture for month-long experiments, suggesting sedimentation of *Prochlorococcus* cells may be limited. Generally, conceptual models of ocean ecology do not include sinking out of picoplanktonic populations as sinking of individual picoplankton cells is expected to be inconsequential [71]. However, particle aggregation could be stimulated via processes such as sloppy feeding or viral lysate [31, 36]. As viral lysate from picocyanobacteria is labile [72–74] aggregation and sinking could be stimulated indirectly via heterotrophic bacterial growth. Particle attachment and aggregation could also be stimulated by TEP (Transparent exopolymer particles), which is produced in xenic *Prochlorococcus* cultures [75, 76]. TEP production appears to be stimulated by high light intensity, characteristic of the surface ocean, and its production appears to be linked to loss rates [75]. Another hypothesis is that export of picoplankton could be attributed to mineral ballasting [71] as both *Synechococcus* [77, 78] and *Prochlorococcus* [78, 79] have been suggested to accumulate biogenic silica.

Physiological stress(es)

Other potential loss mechanisms include physiological stress which can be induced, for example, by high-level irradiance associated with ultraviolet radiation [80, 81] and refraction of light through surface waves that could lead to photodamage via the flashing effect [82, 83]. Other abiotic factors such as nutrient deficiency [84], metal toxicity [85–87], and thermal variations [88, 89] can also contribute to increased stress, though we do not expect significant thermal variations to be important in the NPSG (mean seasonal changes are +/- 3°C (23.5-26.5 °C)). Stresses often result in the generation of reactive oxygen species, that cause oxidative stress and can lead to DNA damage. Reactive oxygen species are also used as a signalling pathway for programmed cell death in photosynthetic microbes [90–92], though there is a lack of evidence for a programmed cell death pathway in *Prochlorococcus* and sympatric heterotrophic bacteria are thought to alleviate this type of stress [93, 94]. We note that there is also a lack of evidence for toxin-antitoxin systems, which are typically common across bacteria and archaea and could act as a pathway to additional cell loss, in *Prochlorococcus* [95].

Population heterogeneity

Microbes experience senescence and aging, leading to intracellular accumulation of damage through their life cycle [96], which may lead to asymmetric division [97]. Unlike other microorganisms, *Prochlorococcus* does not have resting stages and rely on heterotrophic bacteria to survive nutrient starvation in cultures [98], though the types of heterotrophic bacteria they form associations with *in situ* differ from those found in culture which tend to be copiotrophic [99]. *Prochlorococcus* populations are combinations of ecotypes which respond differently to environmental stressors [100–105]. Heterogeneity within the *Prochlorococcus* population, potentially via vertical displacement, may mean there are differing mortality responses at the individual or strain-level vs. at the scale of total population. Additionally, competition between ecotypes and with other phytoplankton in the same niche (like *Synechococcus* or picoeukaryotes) may also increase stresses, especially in an oligotrophic environment like the NPSG where nutrients are limited.

Overall, the fit of model dynamics to NPSG measurements enabled us to examine how much of *Prochlorococcus* mortality can be ascribed to viral lysis, heterotrophic nanoflagellate grazing, or other loss processes. In partitioning *Prochlorococcus* mortality, we found different outcomes across the different model scenarios and independent auxiliary estimates (Figure 5). Indirect estimates via encounter rate or quota-based theory are poorly constrained and are limited by our current knowledge of microbial ecological life-history traits. However, fitting the ECLIP dynamical models, to the data resulted in more constrained mortality estimates. These results mean that viral-induced mortality of *Prochlorococcus* in this system on diel time scales is relatively weak, consistent with prior estimates [23]. Low levels of viral-induced mortality have also been found for *Prochlorococcus* and *Synechococcus* in the Sargasso Sea [106], and the Mediterranean and Red Sea [23]. This could be a defining characteristic of viral impacts on cyanobacteria in oligotrophic gyres – as opposed to more dynamic ocean regions where viral mortality can be considerably more substantial [107, 108]. We note that the ECLIP models predicted that other sources of mortality were likely important in explaining community diel patterns.

We found that direct estimates of mortality from grazing incubation experiments and infected cell measurements also provide evidence that heterotrophic nanoflagellate grazing and T4- and T7- like viral-induced mortality do not account for all *Prochlorococcus* losses in the NPSG. Quantifying the relative importance of mortality processes beyond conventional top-down effects (grazing and lysis) is critical for understanding how grazers and viruses contribute to mortality and energy transfer in marine microbial communities [2, 26, 27, 31]. Interestingly, our analysis of FLB experimental data suggested lower levels of grazing mortality compared to those inferred via ECLIP. Potential reasons for this difference may be reflective of assumptions made in our interpretation of FLB data, could be related to the experimental conditions grazers are subjected to within FLB uptake experiments, or might suggest that grazers do not uptake this biological tracer at the same rate as *Prochlorococcus* – which may reflect differences in chemical composition, size, or infection status [24].

The finding that model-data fits impute other sources of mortality as quantitatively significant suggests that we may be not be accounting for all important feedback mechanisms in our representation of marine surface community dynamics. A missing component in our modelling framework is the effects of mixotrophic nanoflagellates [24, 65, 67, 109, 110] which are likely the main source of additional losses. We did not include mixotrophs in our inference framework due to experimental difficulties in separating phototrophic from mixotrophic nanoflagellates, and due to theoretical challenges in terms of appropriate physiological modelling. However, losses of phytoplankton from the surface oceans are likely to include factors beyond grazing and viral-induced lysis [111, 112]. In Box 1 we review some potential mechanisms that may contribute to the unaccounted losses of *Prochlorococcus*, including ecological feedbacks that lead to distinct functional and/or light-driven responses, aggregation and/or sinking, stress, population heterogeneity, as well as the possibility of having missed other significant sources of top-down mortality (e.g., grazing by mixotrophs [24, 67], or larger organisms; or uncharacterized viral infections [68]). Similarly, our measurements may miss heterogeneities within the *Prochlorococcus* population that mask our ability to interpret mortality. Alternatively, we may be missing entire mechanisms of loss such as via particle aggregation and sinking out, or via physiological stresses on cells. Investigating whether alternative mechanisms of *Prochlorococcus* losses could be significant warrants future research, and may be critical to improving understanding of how biomass and nutrients are transferred through marine food webs. Further investigation and characterization of growth dynamics may also be warranted, as a mischaracterization of growth dynamics may impact our abilities to infer mortality processes – note, at depth *Prochloroccocus* has recently been shown to rely on mixotrophic strategies [113].

The ECLIP modelling framework also comes with caveats, despite the inclusion of multiple populations and interactions. First, we have focused on the impacts of direct, light-driven forcing of cyanobacterial division – hence, oscillations arising in other components reflect a combination of instabilities that can arise in nonlinear population models as well as the cascading impacts of such oscillations on the com-

munity. Unlike other modelling efforts focused on picoplankton which include generic loss terms, e.g. [2, 11, 13, 114, 115], ECLIP can be used to infer how losses are partitioned between grazing, lysis, and other processes. On the other hand ECLIP does not explicitly capture size-structured processes which are important drivers of growth [2, 11, 13, 114, 115] and other ecological interactions [17]. Additionally, light-driven forcing of division does not fully account for light-driven and diurnal-timescale variability in processes such as nutrient content [60, 116, 117], and metabolic state [60]. While these attributes are not specifically modeled, they may have bearing on the values of life-history trait parameters. ECLIP provides a complementary framework for understanding marine microbial ecology; and we hope future efforts will attempt to blend these types of models e.g. [118]. Direct incorporation of diel impacts on grazing [19, 21, 24, 119] or viral traits (e.g., adsorption) [22, 120] may be required to mechanistically understand population dynamics on sub-daily timescales – and particularly the magnitude of oscillations, including in infected cell abundances. Second, we have used two focal processes to examine ways that carbon and other nutrients in basal picoplankton are transferred, e.g., up through the food chain via grazing or retained in the microbial loop due to viral lysis (aka the viral shunt) [33, 34]. This dichotomy reflects a potential tension in the extent to which primary production stimulates the biological pump which requires further investigation. Extensions to the current model might also examine the mechanistic process of export explicitly, whether through coupling grazing to the generation of particles and/or examining the extent to which viral lysis generates aggregates which can exported to the deep oceans via the viral shuttle [36, 121]. Finally, our work has identified a potential accounting challenge in quantifying the balance of *Prochlorococcus* growth and losses. Despite the daily growth and division of cells, the overall abundance remains tightly constrained – our work suggests that this constraint may in fact depend on other factors beyond conventional mechanisms of loss ascribed to T4- and T7-like cyanophage and nanoflagellate grazers.

In summary, this multi-trophic modelling framework provides an opportunity to test the limits of our understanding of ecological and physiological feedback mechanisms of microbial communities in the surface open ocean. In doing so, the model has provided additional support for the hypothesis that relatively high viral abundances can be compatible with relatively low infection (and mortality) rates, while also identifying a key direction for future work: identifying the potentially 'missing mortality' of phytoplankton at the base of the marine food web. Moving forward, *in situ* observations will be needed to probe aggregation and sinking, autolysis, programmed cell death, or other forms of loss of *Prochlorococcus* in the surface ocean and to understand the feedbacks of variation in cyanobacterial growth and loss in a changing ocean.

Acknowledgements

We thank the captain and crew of the R/V Kilo Moana for their effort and assistance on the Hawaii Ocean Experiment Legacy II cruise (KM1513); we thank Michael Follows for feedback that helped improve the manuscript, and we thank Jeremy Harris for code review. This work was supported by grants from the Simons Foundation (no. 549894 to J.R.C., no. 721231 to J.S.W, and no. 329108 to E.V.A., D.A.C., D.L., A.E.W. and J.S.W). This is a contribution of the Simons Collaboration on Ocean Processes and Ecology (SCOPE). This research was supported in part through research cyberinfrastructure resources and services provided by the Partnership for an Advanced Computing Environment (PACE) at the Georgia Institute of Technology, Atlanta, Georgia, USA.

Data availability

Code for ECLIP and performing Bayesian parameter inference was written and run in Julia, with plotting performed in MATLAB. Core code for running model simulations, analysis and plotting is archived on Zenodo: https://doi.org/10.5281/zenodo.7388552 [59].

Conflict of interest

The authors declare that they have no conflict of interest.

References

1. Vaulot, D. & Marie, D. Diel variability of photosynthetic picoplankton in the equatorial Pacific. *Journal of Geophysical Research: Oceans* **104,** 3297–3310 (1999).
2. Ribalet, F. *et al.* Light-driven synchrony of *Prochlorococcus* growth and mortality in the subtropical Pacific gyre. *Proceedings of the National Academy of Sciences* **112,** 8008–8012 (2015).
3. Tsakalakis, I., Pahlow, M., Oschlies, A., Blasius, B. & Ryabov, A. B. Diel light cycle as a key factor for modelling phytoplankton biogeography and diversity. *Ecological Modelling* **384,** 241–248 (2018).
4. Hu, S. K., Connell, P. E., Mesrop, L. Y. & Caron, D. A. A hard days night: Diel shifts in microbial eukaryotic activity in the North Pacific Subtropical Gyre. *Frontiers in Marine Science* **5,** 351 (2018).
5. Welkie, D. G. *et al.* A Hard Day's Night: Cyanobacteria in Diel Cycles. *Trends in Microbiology* **27,** 231–242. ISSN: 0966-842X. http://www.sciencedirect.com/science/article/pii/S0966842X1830252X (3 2018).
6. Becker, K. W. *et al.* Daily changes in phytoplankton lipidomes reveal mechanisms of energy storage in the open ocean. *Nature Communications* **9,** 5179 (2018).
7. Hunter-Cevera, K. R. *et al.* Seasons of *Syn*. *Limnology and Oceanography* **65,** 1085–1102 (2020).
8. Malerba, M. E., Marshall, D. J., Palacios, M. M., Raven, J. A. & Beardall, J. Cell size influences inorganic carbon acquisition in artificially selected phytoplankton. *New Phytologist* (2020).
9. Li, C. *et al.* Quasi-antiphase Diel Patterns of Abundance and Cell Size/Biomass of Picophytoplankton in the Oligotrophic Ocean. *Geophysical Research Letters* **49,** e2022GL097753 (2022).
10. Tsakalakis, I., Follows, M. J., Dutkiewicz, S., Follett, C. L. & Vallino, J. J. Diel light cycles affect phytoplankton competition in the global ocean. *Global Ecology and Biogeography* **31,** 1838–1849. eprint: https://onlinelibrary.wiley.com/doi/pdf/10.1111/geb.13562. https://onlinelibrary.wiley.com/doi/abs/10.1111/geb.13562 (2022).
11. Mattern, J. P. *et al.* A Bayesian approach to modeling phytoplankton population dynamics from size distribution time series. *PLoS Computational Biology* **18,** e1009733 (2022).
12. Sosik, H. M., Olson, R. J., Neubert, M. G., Shalapyonok, A. & Solow, A. R. Growth rates of coastal phytoplankton from time-series measurements with a submersible flow cytometer. *Limnology and Oceanography* **48,** 1756–1765 (2003).
13. Hunter-Cevera, K. R. *et al.* Diel size distributions reveal seasonal growth dynamics of a coastal phytoplankter. *Proceedings of the National Academy of Sciences* **111,** 9852–9857 (2014).
14. Taniguchi, D. A., Franks, P. J. & Poulin, F. J. Planktonic biomass size spectra: an emergent property of size-dependent physiological rates, food web dynamics, and nutrient regimes. *Marine Ecology Progress Series* **514,** 13–33 (2014).
15. Acevedo-Trejos, E., Brandt, G., Smith, S. L. & Merico, A. PhytoSFDM version 1.0. 0: phytoplankton size and functional diversity model. *Geoscientific Model Development* **9,** 4071–4085 (2016).
16. Chen, B. & Smith, S. L. CITRATE 1.0: Phytoplankton continuous trait-distribution model with one-dimensional physical transport applied to the North Pacific. *Geoscientific Model Development* **11,** 467–495 (2018).
17. Talmy, D. *et al.* Contrasting controls on microzooplankton grazing and viral infection of microbial prey. *Frontiers in Marine Science* **6,** 182 (2019).
18. De Corte, D., Paredes, G., Yokokawa, T., Sintes, E. & Herndl, G. J. Differential response of *Cafeteria roenbergensis* to different Bacterial and Archaeal prey characteristics. *Microbial Ecology* **78,** 1–5. ISSN: 1432-184X. https://doi.org/10.1007/s00248-018-1293-y (2019).
19. Ng, W. H. A. & Liu, H. Diel periodicity of grazing by heterotrophic nanoflagellates influenced by prey cell properties and intrinsic grazing rhythm. *Journal of Plankton Research* **38,** 636–651 (2016).
20. Aylward, F. O. *et al.* Diel cycling and long-term persistence of viruses in the oceans euphotic zone. *Proceedings of the National Academy of Sciences* **114,** 11446–11451 (2017).

21. Arias, A., Saiz, E. & Calbet, A. Towards an Understanding of Diel Feeding Rhythms in Marine Protists: Consequences of Light Manipulation. *Microbial Ecology* **79,** 64–72. ISSN: 1432-184X. https://doi.org/10.1007/s00248-019-01390-y (2020).

22. Demory, D. *et al.* Linking light-dependent life history traits with population dynamics for *Prochlorococcus* and cyanophage. *mSystems* **5,** e00586–19 (2020).

23. Mruwat, N. *et al.* A single-cell polony method reveals low levels of infected *Prochlorococcus* in oligotrophic waters despite high cyanophage abundances. *The ISME Journal* **15,** 41–54 (2021).

24. Connell, P. E., Ribalet, F., Armbrust, E. V., White, A. E. & Caron, D. A. Diel oscillations in feeding strategies of heterotrophic and mixotrophic nanoplankton in the North Pacific Subtropical Gyre. *Aquatic Microbial Ecology* **85,** 167–181 (2020).

25. Partensky, F., Hess, W. R. & Vaulot, D. *Prochlorococcus*, a marine photosynthetic prokaryote of global significance. *Microbiology and Molecular Biology Reviews* **63,** 106–127 (1999).

26. Pasulka, A. L., Samo, T. J. & Landry, M. R. Grazer and viral impacts on microbial growth and mortality in the southern California Current Ecosystem. *Journal of Plankton Research* **37,** 320–336 (2015).

27. Mojica, K. D., Huisman, J., Wilhelm, S. W. & Brussaard, C. P. Latitudinal variation in virus-induced mortality of phytoplankton across the North Atlantic Ocean. *The ISME Journal* **10,** 500 (2016).

28. Beckett, S. J. & Weitz, J. S. Disentangling niche competition from grazing mortality in phytoplankton dilution experiments. *PLOS ONE* **12,** e0177517 (2017).

29. Calbet, A. & Saiz, E. How much is enough for nutrients in microzooplankton dilution grazing experiments? *Journal of Plankton Research* **40,** 109–117 (2017).

30. Beckett, S. J. & Weitz, J. S. The effect of strain level diversity on robust inference of virus-induced mortality of phytoplankton. *Frontiers in Microbiology* **9,** 1850 (2018).

31. Talmy, D. *et al.* An empirical model of carbon transfer to marine viruses and zooplankton grazers. *Environmental Microbiology* **21,** 2171–2181 (2019).

32. Azam, F. *et al.* The ecological role of water-column microbes in the sea. *Marine ecology progress series,* 257–263 (1983).

33. Fuhrman, J. A. Marine viruses and their biogeochemical and ecological effects. *Nature* **399,** 541–548 (1999).

34. Wilhelm, S. W. & Suttle, C. A. Viruses and nutrient cycles in the sea: viruses play critical roles in the structure and function of aquatic food webs. *Bioscience* **49,** 781–788 (1999).

35. Weitz, J. S. & Wilhelm, S. W. Ocean viruses and their effects on microbial communities and biogeochemical cycles. *F1000 biology reports* **4** (2012).

36. Sullivan, M. B., Weitz, J. S. & Wilhelm, S. Viral ecology comes of age. *Environmental Microbiology Reports* **9,** 33–35 (2017).

37. Breitbart, M., Bonnain, C., Malki, K. & Sawaya, N. A. Phage puppet masters of the marine microbial realm. *Nature microbiology* **3,** 754–766 (2018).

38. Weitz, J. S. *et al.* A multitrophic model to quantify the effects of marine viruses on microbial food webs and ecosystem processes. *The ISME Journal* **9,** 1352 (2015).

39. Mateus, M. D. Bridging the Gap between Knowing and Modeling Viruses in Marine Systems–An Upcoming Frontier. *Frontiers in Marine Science* **3,** 284 (2017).

40. Grossowicz, M. *et al. Prochlorococcus* in the lab and *in silico*: the importance of representing exudation. *Limnology and Oceanography* **62,** 818–835 (2017).

41. Middleton, J. E., Martnez Martnez, J., Wilson, W. H. & Record, N. R. Functional dynamics of *Emiliania huxleyi* virus-host interactions across multiple spatial scales. *Limnology and Oceanography* **62,** 922–933 (2017).

42. Wirtz, K. W. Physics or biology? Persistent chlorophyll accumulation in a shallow coastal sea explained by pathogens and carnivorous grazing. *PLOS ONE* **14,** e0212143 (2019).

43. Xie, L., Zhang, R. & Luo, Y.-W. Assessment of Explicit Representation of Dynamic Viral Processes in Regional Marine Ecological Models. *Viruses* **14,** 1448 (2022).

44. Frias-Lopez, J., Thompson, A., Waldbauer, J. & Chisholm, S. W. Use of stable isotope-labelled cells to identify active grazers of picocyanobacteria in ocean surface waters. *Environmental Microbiology* **11,** 512–525 (2009).

45. Caron, D. A. Acknowledging and incorporating mixed nutrition into aquatic protistan ecology, finally. *Environmental Microbiology Reports* **9,** 41–43 (2017).

46. Binder, B. J. & DuRand, M. D. Diel cycles in surface waters of the equatorial Pacific. *Deep Sea Research Part II: Topical Studies in Oceanography* **49,** 2601–2617 (2002).

47. Berube, P. M., Rasmussen, A., Braakman, R., Stepanauskas, R. & Chisholm, S. W. Emergence of trait variability through the lens of nitrogen assimilation in *Prochlorococcus*. *Elife* **8,** e41043 (2019).

48. Ribalet, F. *et al.* SeaFlow data v1: High-resolution abundance, size and biomass of small phytoplankton in the North Pacific. Version 1.2. *Zenodo* **doi: 10.5281/zenodo.3445407.** https://doi.org/10.5281/zenodo.3445407 (June 2019).

49. Ribalet, F. *et al.* SeaFlow data v1, high-resolution abundance, size and biomass of small phytoplankton in the North Pacific. *Scientific Data* **6,** 1–8 (2019).

50. Freitas, F. H. *et al.* Diel variability of bulk optical properties associated with the growth and division of small phytoplankton in the North Pacific Subtropical Gyre. *Applied Optics* **59,** 6702–6716 (2020).

51. Ashkezari, M. D. *et al.* Simons collaborative marine atlas project (Simons CMAP): an open-source portal to share, visualize, and analyze ocean data. *Limnology and Oceanography: Methods* **19,** 488–496 (2021).

52. Baran, N., Goldin, S., Maidanik, I. & Lindell, D. Quantification of diverse virus populations in the environment using the polony method. *Nature Microbiology* **3,** 62–72 (2018).

53. Goldin, S., Hulata, Y., Baran, N. & Lindell, D. Quantification of T4-like and T7-like cyanophages using the polony method show they are significant members of the virioplankton in the photic zone of the North Pacific Subtropical Gyre. *Frontiers in Microbiology* **11,** 1210 (2020).

54. Sherr, E. B., Caron, D. A. & Sherr, B. F. *Staining of heterotrophic protists for visualization via epifluorescence microscopy* 213–227 (Lewis Publishers, Boca Raton, 1993).

55. Ge, H., Xu, K. & Ghahramani, Z. *Turing: a language for flexible probabilistic inference* in *International Conference on Artificial Intelligence and Statistics, AISTATS 2018, 9-11 April 2018, Playa Blanca, Lanzarote, Canary Islands, Spain* (2018), 1682–1690. http://proceedings.mlr.press/v84/ge18b.html.

56. Bezanson, J., Edelman, A., Karpinski, S. & Shah, V. B. Julia: A fresh approach to numerical computing. *SIAM review* **59,** 65–98. https://doi.org/10.1137/141000671 (2017).

57. Lambert, B. *A students guide to Bayesian statistics* (Sage, 2018).

58. Hoffman, M. D., Gelman, A., *et al.* The No-U-Turn sampler: adaptively setting path lengths in Hamiltonian Monte Carlo. *J. Mach. Learn. Res.* **15,** 1593–1623 (2014).

59. Beckett, S. *et al. Code for: Diel population dynamics and mortality of Prochlorococcus in the North Pacific Subtropical Gyre* version ECLIP. Dec. 2022. https://doi.org/10.5281/zenodo.7388552.

60. Muratore, D. *et al.* Complex marine microbial communities partition metabolism of scarce resources over the diel cycle. *Nature Ecology & Evolution* **6,** 218–229 (2022).

61. Christaki, U., Giannakourou, A., Van Wambeke, F. & Grégori, G. Nanoflagellate predation on auto-and heterotrophic picoplankton in the oligotrophic Mediterranean Sea. *Journal of Plankton Research* **23,** 1297–1310 (2001).

62. Gutenkunst, R. N. *et al.* Universally sloppy parameter sensitivities in systems biology models. *PLoS computational biology* **3,** e189 (2007).

63. Boenigk, J. & Arndt, H. Bacterivory by heterotrophic flagellates: community structure and feeding strategies. *Antonie Van Leeuwenhoek* **81,** 465–480 (2002).

64. Labarre, A., Obiol, A., Wilken, S., Forn, I. & Massana, R. Expression of genes involved in phagocytosis in uncultured heterotrophic flagellates. *Limnology and Oceanography* **65,** S149–S160 (2020).

65. Li, Q., Edwards, K. F., Schvarcz, C. R., Selph, K. E. & Steward, G. F. Plasticity in the grazing ecophysiology of *Florenciella* (Dichtyochophyceae), a mixotrophic nanoflagellate that consumes *Prochlorococcus* and other bacteria. *Limnology and Oceanography* **66,** 47–60 (2021).

66. Zubkov, M. V. & Tarran, G. A. High bacterivory by the smallest phytoplankton in the North Atlantic Ocean. *Nature* **455,** 224–226 (2008).

67. Li, Q., Edwards, K. F., Schvarcz, C. R. & Steward, G. F. Broad phylogenetic and functional diversity among mixotrophic consumers of *Prochlorococcus*. *The ISME journal* **16,** 1557–1569 (2022).

68. Cai, L. *et al.* Abundant and cosmopolitan lineage of cyanopodoviruses lacking a DNA polymerase gene. *The ISME Journal,* 1–11. ISSN: 1751-7362 (2022).

69. Richardson, T. L. & Jackson, G. A. Small phytoplankton and carbon export from the surface ocean. *Science* **315,** 838–840 (2007).

70. Guidi, L. *et al.* Plankton networks driving carbon export in the oligotrophic ocean. *Nature* **532,** 465 (2016).

71. Richardson, T. L. Mechanisms and pathways of small-phytoplankton export from the surface ocean. *Ann. Rev. Mar. Sci* **11,** 57–74 (2019).

72. Zhao, Z. *et al.* Microbial transformation of virus-induced dissolved organic matter from picocyanobacteria: coupling of bacterial diversity and DOM chemodiversity. *The ISME Journal* **13,** 2551–2565 (2019).

73. Xiao, X. *et al.* Viral lysis alters the optical properties and biological availability of dissolved organic matter derived from picocyanobacteria *Prochlorococcus*. *Applied and Environmental Microbiology* **87,** e02271–20. ISSN: 0099-2240. eprint: https://aem.asm.org/content/early/2020/11/09/AEM.02271-20.full.pdf. https://aem.asm.org/content/early/2020/11/09/AEM.02271-20 (2021).

74. Zheng, Q. *et al.* Highly enriched N-containing organic molecules of *Synechococcus* lysates and their rapid transformation by heterotrophic bacteria. *Limnology and Oceanography* **66,** 335–348 (2021).

75. Iuculano, F., Mazuecos, I. P., Reche, I. & Agust, S. *Prochlorococcus* as a possible source for transparent exopolymer particles (TEP). *Frontiers in Microbiology* **8,** 709 (2017).

76. Cruz, B. N. & Neuer, S. Heterotrophic bacteria enhance the aggregation of the marine picocyanobacteria *Prochlorococcus* and *Synechococcus*. *Frontiers in Microbiology* **10,** 1864 (2019).

77. Baines, S. B. *et al.* Significant silicon accumulation by marine picocyanobacteria. *Nature Geoscience* **5,** 886–891 (2012).

78. Krause, J. W. *et al.* Picoplankton contribution to biogenic silica stocks and production rates in the Sargasso Sea. *Global Biogeochemical Cycles* **31,** 762–774 (2017).

79. Wei, Y. *et al.* Significant contribution of picoplankton size fraction to biogenic silica standing stocks in the Western Pacific Ocean. *Progress in Oceanography* **192,** 102516 (2021).

80. Llabrés, M., Agust, S. & Herndl, G. J. Diel in situ picophytoplankton cell death cycles coupled with cell division. *Journal of phycology* **47,** 1247–1257 (2011).

81. Mella-Flores, D. *et al.* *Prochlorococcus* and *Synechococcus* have evolved different adaptive mechanisms to cope with light and UV stress. *Frontiers in Microbiology* **3,** 285 (2012).

82. Stramska, M. & Dickey, T. D. Short-term variability of the underwater light field in the oligotrophic ocean in response to surface waves and clouds. *Deep Sea Research Part I: Oceanographic Research Papers* **45,** 1393–1410 (1998).

83. Demory, D. *et al.* How do microalgae perceive light in a high-rate pond? Towards more realistic Lagrangian experiments. *Royal Society open science* **5,** 180523 (2018).

84. Kulk, G., van de Poll, W. H., Visser, R. J. & Buma, A. G. Low nutrient availability reduces high-irradiance-induced viability loss in oceanic phytoplankton. *Limnology and Oceanography* **58,** 1747–1760 (2013).

85. Mann, E. L. & Chisholm, S. W. Iron limits the cell division rate of *Prochlorococcus* in the eastern equatorial Pacific. *Limnology and Oceanography* **45,** 1067–1076 (2000).

86. Mann, E. L., Ahlgren, N., Moffett, J. W. & Chisholm, S. W. Copper toxicity and cyanobacteria ecology in the Sargasso Sea. *Limnology and Oceanography* **47,** 976–988 (2002).

87. Sarker, I., Moore, L. R. & Tetu, S. G. Investigating zinc toxicity responses in marine *Prochlorococcus* and *Synechococcus*. *Microbiology* **167,** 001064 (2021).

88. Pittera, J. *et al.* Connecting thermal physiology and latitudinal niche partitioning in marine *Synechococcus*. *The ISME Journal* **8,** 1221 (2014).

89. Baker, K. G. & Geider, R. J. Phytoplankton mortality in a changing thermal seascape. *Global Change Biology* **27,** 5253–5261 (2021).

90. Vardi, A. *et al.* A stress surveillance system based on calcium and nitric oxide in marine diatoms. *PLOS Biology* **4,** e60 (2006).

91. Bidle, K. D. The molecular ecophysiology of programmed cell death in marine phytoplankton. *Annual review of marine science* **7,** 341–375 (2015).

92. Bidle, K. D. Programmed cell death in unicellular phytoplankton. *Current Biology* **26,** R594–R607 (2016).

93. Morris, J. J., Kirkegaard, R., Szul, M. J., Johnson, Z. I. & Zinser, E. R. Facilitation of robust growth of *Prochlorococcus* colonies and dilute liquid cultures by helper heterotrophic bacteria. *Applied and Environmental Microbiology* **74,** 4530–4534 (2008).

94. Morris, J. J., Johnson, Z. I., Szul, M. J., Keller, M. & Zinser, E. R. Dependence of the cyanobacterium *Prochlorococcus* on hydrogen peroxide scavenging microbes for growth at the ocean's surface. *PLOS ONE* **6,** e16805 (2011).

95. Fucich, D. & Chen, F. Presence of toxin-antitoxin systems in picocyanobacteria and their ecological implications. *The ISME Journal* **14,** 2843–2850 (2020).

96. Moger-Reischer, R. Z. & Lennon, J. T. Microbial ageing and longevity. *Nature Reviews Microbiology* **17,** 679–690 (2019).

97. Franklin, D. J. Explaining the causes of cell death in cyanobacteria: what role for asymmetric division? *Journal of Plankton Research* **36,** 11–17 (2013).

98. Roth-Rosenberg, D. *et al.* *Prochlorococcus* Cells Rely on Microbial Interactions Rather than on Chlorotic Resting Stages To Survive Long-Term Nutrient Starvation. *mBio* **11** (2020).

99. Kearney, S. M., Thomas, E., Coe, A. & Chisholm, S. W. Microbial Diversity of Co-occurring Heterotrophs in Cultures of Marine Picocyanobacteria. *Environmental Microbiome* **16,** 1 (1 2021).

100. Moore, L. R. & Chisholm, S. W. Photophysiology of the marine cyanobacterium *Prochlorococcus*: ecotypic differences among cultured isolates. *Limnology and Oceanography* **44,** 628–638 (1999).

101. Martiny, A. C., Coleman, M. L. & Chisholm, S. W. Phosphate acquisition genes in *Prochlorococcus* ecotypes: evidence for genome-wide adaptation. *Proceedings of the National Academy of Sciences* **103,** 12552–12557 (2006).

102. Tolonen, A. C. *et al.* Global gene expression of *Prochlorococcus* ecotypes in response to changes in nitrogen availability. *Molecular systems biology* **2,** 53 (2006).

103. Johnson, Z. I. *et al.* Niche partitioning among *Prochlorococcus* ecotypes along ocean-scale environmental gradients. *Science* **311,** 1737–1740 (2006).

104. Zinser, E. R. *et al.* Influence of light and temperature on *Prochlorococcus* ecotype distributions in the Atlantic Ocean. *Limnology and Oceanography* **52,** 2205–2220 (2007).

105. Thompson, A. W., Huang, K., Saito, M. A. & Chisholm, S. W. Transcriptome response of high- and low-light-adapted *Prochlorococcus* strains to changing iron availability. *The ISME Journal* **5,** 1580–1594 (2011).

106. Matteson, A. R. *et al.* High abundances of cyanomyoviruses in marine ecosystems demonstrate ecological relevance. *FEMS microbiology ecology* **84,** 223–234 (2013).

107. Fuhrman, J. A. & Noble, R. T. Viruses and protists cause similar bacterial mortality in coastal seawater. *Limnology and oceanography* **40,** 1236–1242 (1995).

108. Carlson, M. *et al.* Viruses affect picocyanobacterial abundance and biogeography in the North Pacific Ocean. *Nature microbiology* **7,** 570–580 (2022).

109. Sanders, R. W. & Porter, K. G. in *Advances in microbial ecology* 167–192 (Springer, 1988).

110. Stoecker, D. K., Hansen, P. J., Caron, D. A. & Mitra, A. Mixotrophy in the marine plankton. *Annu. Rev. Mar. Sci* **9,** 311–335 (2017).

111. Brum, J. R., Morris, J. J., Décima, M. & Stukel, M. R. Mortality in the oceans: causes and consequences. *Association for the Sciences of Limnology and Oceanography,* 16–48 (2014).

112. Aguilera, A. *et al.* Cell death in Cyanobacteria: current understanding and recommendations for a consensus on its nomenclature. *Frontiers in Microbiology* **12** (2021).

113. Wu, Z. *et al.* Single-cell measurements and modelling reveal substantial organic carbon acquisition by *Prochlorococcus*. *Nature Microbiology,* 1–10 (2022).

114. Hynes, A. M., Blythe, B. J. & Binder, B. J. An individual-based model for the analysis of *Prochlorococcus* diel cycle behavior. *Ecological Modelling* **301,** 1–15 (2015).

115. Hynes, A. M., Rhodes, K. L. & Binder, B. J. Assessing cell cycle-based methods of measuring *Prochlorococcus* division rates using an individual-based model. *Limnology and Oceanography: Methods* **13,** 640–650 (2015).

116. Lopez, J. S., Garcia, N. S., Talmy, D. & Martiny, A. C. Diel variability in the elemental composition of the marine cyanobacterium *Synechococcus*. *Journal of Plankton Research* **38,** 1052–1061 (2016).

117. Vislova, A., Sosa, O. A., Eppley, J. M., Romano, A. E. & DeLong, E. F. Diel oscillation of microbial gene transcripts declines with depth in oligotrophic ocean waters. *Frontiers in microbiology* **10,** 2191 (2019).

118. Beckett, S. J. *et al.* Diel population dynamics and mortality of *Prochlorococcus* in the North Pacific Subtropical Gyre. *bioRxiv* (2021).

119. Groussman, R. D., Coesel, S. N., Durham, B. P. & Armbrust, E. V. Diel-Regulated Transcriptional Cascades of Microbial Eukaryotes in the North Pacific Subtropical Gyre. *Frontiers in microbiology* **12** (2021).

120. Thamatrakoln, K. *et al.* Light regulation of coccolithophore host–virus interactions. *New Phytologist* **221,** 1289–1302 (2018).

121. Weinbauer, M. G. Ecology of prokaryotic viruses. *FEMS Microbiology Reviews* **28,** 127–181 (2004).

Supplementary Information for

Diel population dynamics and mortality of *Prochlorococcus* in the North Pacific Subtropical Gyre

S1 Alternative mortality estimates

S1.1 Modelling encounter rates and allometry

S1.1.1 Viral encounter rate

Both *Prochlorococcus* and their viruses diffuse and the rates at which they may encounter each other can be estimated using biophysical models [1–3]. We assume the maximum encounter rate between diffusing spherical particles of two different sizes, r_{virus} and r_{cell} is given by the Smoulouski equation [4]. However, an encounter does not always lead to adsorption [1, 5] so we subject the maximum encounter rate to an efficiency of encounter term, ϵ_ϕ, as:

$$\phi(r_{virus}, r_{cell}) = \epsilon_\phi \left(4\pi \left(D_{cell} + D_{virus}\right)\left(r_{virus} + r_{cell}\right)\right) \tag{S1}$$

where diffusion of each spherical particle of radius r is given by the classical relation[6]:

$$D(r_d) = \frac{K_b \cdot T}{6\pi \cdot \rho \cdot r_d} \tag{S2}$$

with K_b, the Boltzmann constant, T is temperature (in Kelvin) and ρ is the dynamic viscosity of the medium. We assume $T = 25°\text{C}$ [7] and $\rho = 9.96 \times 10^{-10}$ kg μm^{-1} s^{-1} [1]. We assume that free viruses can adsorb to both susceptible and infected *Prochlorococcus* cells. Both cases result in losses of free virus particles. Susceptible cells that viruses adsorb to become infected. However, we assume that viruses that adsorb to infected cells do not alter the physiological responses of infected cells. As radius scales as $\approx [\text{volume}]^{1/3}$, both diffusion and encounter rate are size-dependent [1].

S1.1.2 Grazer encounter rate

We estimated encounter rates between grazers and prey by modelling the volume of water a swimming grazer will encounter as:

$$\psi = u\pi R^2 \tag{S3}$$

where u is the swimming speed and R is the perception radius of the grazer. Here, the modelled phytoplankton, *Prochlorococcus* do not swim [8, 9]. We further account for differences in predator and prey size and encounter efficiency as:

$$\psi(r_{grazer}, r_{cell}) = \overbrace{\epsilon_\psi}^{encounter\ efficiency} \left(\overbrace{u(r_{grazer})}^{swimming\ speed} \ \pi(\overbrace{f_{detect} r_{grazer} + r_{cell}}^{sensing\ radius})^2 \right) \tag{S4}$$

where we assume grazers swimming speed (μm d^{-1}) scales as a function of grazer equivalent spherical radius (μm) using the empirical relation derived by Kiørboe [10] as:

$$u(r_{grazer}) = 864 \times 10^{(6+u_1)} \left(\frac{2r_{grazer}}{10^4}\right)^{u_2} \tag{S5}$$

with coefficients $u_1 = 0.39$ and $u_2 = 0.79$. We assume grazers detect prey within a detection sensing radius which is proportional to grazer radius with factor $f_{detect} = 3$ [1]. We also incorporate prey size into the perception radius [11].

S1.1.3 Modelling carbon allometry

Ribalet et al., [12] correlate light-scattering to cell size and cell carbon quota using Mie theory. We define cellular elemental quotas (μg per cell) for carbon, C_S as:

$$C_S([\text{volume}]) = 220[\text{volume}] \cdot 10^{-9} \tag{S6}$$

We assume that both infected and susceptible cells have the same elemental quotas. That is $C_I = C_S$.

For the purposes of converting consumed biomass to grazer abundance we assume grazer quotas in μg per cell for carbon, based on the empirical relationship derived by Menden-Deuer and Lessard [13] for dinoflagellates as:

$$C_G(r_{grazer}) = 10^{-6} \cdot 0.76 \left(\frac{4}{3}\pi r_{grazer}^3\right)^{0.819} \tag{S7}$$

S1.2 Viral lysis estimates

S1.2.1 iPolony estimates:

Estimates for viral-induced lysis based on infected cell data recorded on the cruise using the iPolony method are 0.35-4.8% [14], assuming 1-3 infection cycles occur during the turnover time for *Prochlorococcus* cells.

S1.2.2 Viral encounter estimates

Naïve encounter rate estimates are made using the encounter rate theory outlined in equation S1 with baseline parameters assuming that total *Prochlorococcus* loss rates (ω) are between 0.3 and 1 per day. Note that this encounter rate estimation assumes instantaneous killing of *Prochlorococcus*. Assuming that the steady state abundance of T4- and T7-like cyanophages during the cruise was $V^* = 3.5 \times 10^8$ per L, and assuming variation in $\epsilon_\phi \in [10^{-5}, 10^0]$, $r_{virus} \in [20, 50]$ nm, $r_{cell} \in [0.17, 0.49]\mu$m, we find the proportion of *Prochlorococcus* losses via viral-induced lysis can be estimated as:

$$p_{vir} = \frac{\phi(r_{virus}, r_{cell})V^*}{\omega}. \tag{S8}$$

S1.3 Grazing estimates

S1.3.1 Grazer encounter estimates

Naïve encounter rate estimates are made using the encounter rate theory outlined in equation S4 with baseline parameters assuming that total *Prochlorococcus* loss rates (ω) are between 0.3 and 1 per day. Note that this encounter rate estimation assumes instantaneous killing of *Prochlorococcus*. Assuming that the steady state abundance of heterotrophic nanoflagellates during the cruise was $G^* = 2.5 \times 10^5$ per L, and assuming parameter variation in $\epsilon_\psi \in [10^{-5}, 10^0]$, $f_{detect} \in [0, 6]$, $r_{grazer} \in [1, 10]\mu$m, $r_{cell} \in [0.17, 0.49]\mu$m, we estimate the proportion of *Prochlorococcus* losses via grazing as:

$$p_{graz} = \frac{\psi(r_{grazer}, r_{cell})G^*}{\omega}. \tag{S9}$$

S1.3.2 Carbon quota and predator growth rate estimate

Following Connell et al. [15] we use literature values to assume that heterotrophic nanoflagellate growth rate ξ is between 0.2 and 1.4 per day [16–18]. We can write an approximation for the growth rate of the heterotrophic nanoflagellate population, supposing that they only feed on *Prochlorococcus* cells, as:

$$\xi G = \epsilon \frac{C_S}{C_G} \psi \left(S + I\right) G \tag{S10}$$

which can be rearranged to estimate the grazing clearance rate as:

$$\psi = \frac{\xi C_G}{\epsilon C_S \left(S + I\right)}. \tag{S11}$$

We use a steady state approximation of $P^* = S^* + I^* = 1.75 \times 10^8$ *Prochlorococcus* cells per L and a steady state assumption of $G^* = 2.5 \times 10^5$ heterotrophic nanoflagellates per L during the cruise. Assuming variation in $\epsilon \in [0.2, 0.6]$, C_S and C_G we calculate the proportion of losses attributed to grazing as:

$$p_{graz} = \frac{\psi G^*}{\omega} \tag{S12}$$

where ω represents total *Prochlorococcus* loss rates that we assume are between 0.3 and 1 per day.

S1.3.3 FLB estimates

We used Fluorescently Labelled Bacteria (FLB) incubation experiments performed on the cruise [15] to estimate grazing mortality. These experiments measured the proportion of heterotrophic nanoflagellates containing FLB cells after an hour incubation. The proportion of heterotrophic nanoflagellates containing FLB showed diel variability and varied between 1-25% [15]. In order to use these measurements as the basis for estimating grazing mortality we propose that the population dynamics of FLB cells within incubation experiments can be modelled as:

$$\frac{dF}{dt} = -\alpha F G = -AF \tag{S13}$$

where F is the abundance of FLB cells, α is the clearance rate of heterotrophic nanoflagellates feeding on FLB and A represents the grazing rate by heterotrophic nanoflagellates. Assuming that heterotrophic nanoflagellates graze on *Prochlorococcus* and FLB at the same rate, and assuming a constant heterotrophic nanoflagellate population, G, of 2×10^5 cells/L allows a grazing rate A to be computed as:

$$A = -\frac{1}{\tau}\log\left(\frac{F_E}{F_0}\right) \tag{S14}$$

where τ is the experiment length (1 hour), the initial FLB abundance is $F_0 = 10^8$ cells per L, and the final FLB abundance is F_E. Assuming the observed proportion (0.01-0.25) of heterotrophic nanoflagellates containing FLB (Y) consume X FLB on average during the incubation period, we can calculate the final FLB abundance as:

$$F_E = F_0 - XYG. \tag{S15}$$

We assume that X varies between 1 and 25, but, it is unclear exactly how many FLB were eaten per grazer during the 1 hour incubation. We assume that estimated grazing rates on FLB are equivalent to grazing rates on *Prochlorococcus*. To convert to mortality, we assume that total *Prochlorococcus* loss rates, ω are between 0.3 and 1 per day and calculate proportional losses by grazing as:

$$p_{graz} = \frac{A}{\omega} \tag{S16}$$

S2 ECLIP model and parameter inference

For completeness, and to help the reader, we repeat our descriptions of the ECLIP model in the supplementary text.

S2.1 ECLIP: Ecological Community driven by Light, with Infection of Phytoplankton

The ECLIP model represents *Prochlorococcus* division and death where division is light-driven (where cell division is expected to occur at night [19, 20]) and death is controlled by viral lysis, grazing, and other density-dependent factors (Figure 1a). The *Prochlorococcus* population is structured by two states of infection: cells that are susceptible to viral infection (S) and cells that are infected (I) by viruses (V). Grazers (G) feed indiscriminately on both S and I classes. The dynamics of S, I, V and G numerical abundances over time are described by the following system:

$$\begin{aligned}
\frac{dS}{dt} &= \overbrace{\mu(t)S}^{division} - \overbrace{m_P S(S+I)}^{higher\text{-}order\ losses} - \overbrace{\phi S V}^{infection} - \overbrace{\psi S G}^{grazing} \\
\frac{dI}{dt} &= \overbrace{\phi S V}^{infected} - \overbrace{m_P I(S+I)}^{higher\text{-}order} - \overbrace{\eta I}^{viral\text{-}lysis} - \overbrace{\psi I G}^{grazing} \\
\frac{dV}{dt} &= \overbrace{\beta \eta I}^{viral\ production} - \overbrace{\phi(S+I)V}^{adsorption} - \overbrace{m_V V^2}^{higher\text{-}order\ losses} \\
\frac{dG}{dt} &= \overbrace{\epsilon \frac{N_P}{N_G}\psi(S+I)G}^{grazing\ on\ Prochlorococcus} - \overbrace{\gamma G}^{generalist\ grazing} - \overbrace{m_G G^2}^{higher\text{-}order\ losses},
\end{aligned} \tag{S17}$$

where

$$\eta = \frac{24}{LP}, \text{with } LP \text{ is the latent period (in hours)} \tag{S18}$$

$$\mu(t) = \mu_{ave}\,(\ 1\ +\ \delta_\mu \sin(\ 2\pi(t+\delta_t)\ )\ ). \tag{S19}$$

Prochlorococcus have a diel-driven population division rate $\mu(t)$ whose proportional amplitude and phase are set by parameters δ_μ and δ_t, and $t = 0$ represents 06:00:00 local time (see Figure S1). *Prochlorococcus* have a nonlinear loss rate, m_P, dependent on total phytoplankton population size to implicitly represent niche competition [21]. Viruses infect susceptible *Prochlorococcus* at a rate ϕ and create β new virions that are released into the environment upon cellular lysis, which occurs after an infection latent period of $\frac{1}{\eta}$. Grazing upon *Prochlorococcus* is non-preferential with respect to infection status and occurs at a rate ψ with a Gross Growth Efficiency (GGE) ϵ proportional to the fraction of nitrogen contents in a *Prochlorococcus* cell ($N_P = 5.01 \times 10^{-9} \mu$g N cell^{-1}) and a grazer ($N_G = 6.53 \times 10^{-6} \mu$g N cell^{-1}). We introduce γ as a parameter to denote whether grazers act as specialists ($\gamma = 0$) or generalists ($\gamma > 0$), where the term represents net additional gains to the grazer from non-*Prochlorococcus* prey sources after accounting for respiratory costs. Generalist strategies may include ingesting other phytoplankton, heterotrophic bacteria, or other grazers through intraguild predation. Grazer and viral losses are both characterized by a nonlinear loss term to avoid structurally biasing the model to favour one of these types of *Prochlorococcus* predators [22] and to avoid competitive exclusion. A full list of parameters are shown in Table S1.

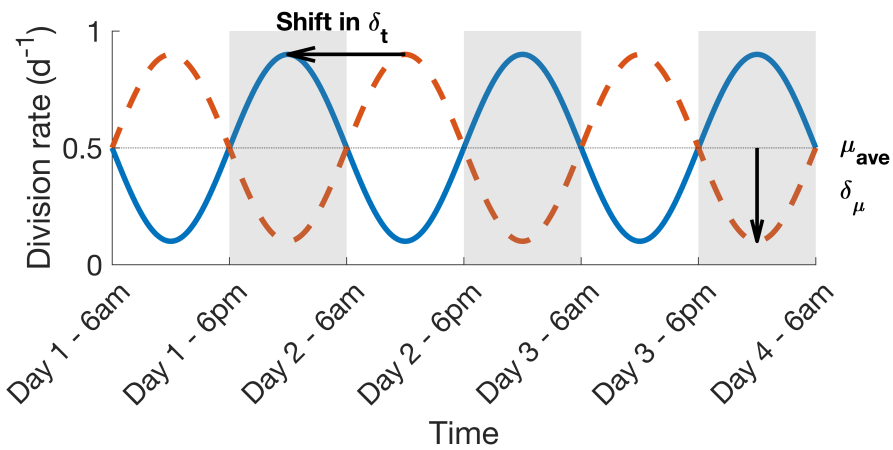

Figure S1: Diel-driven division rate. Solid blue and dashed orange lines are example division rate curves to graphically explain how the different parameters used in the diel-driven division rate function in ECLIP alter the model division rate. The parameters for division rate are represented by the average division rate over 1 day, μ_{ave}, the amplitude of the sinusoidal oscillations, δ_μ, and the phase of the sinusoidal signal, δ_t. The two curves differ in their value of δ_t; the orange curve has $\delta_t = 0$, while $\delta_t = 0.5$ days for the blue curve.

S2.1.1 Defining the specialism-generalism gradient

We define the degree of generalism ($d_{\text{generalism}}$) as the ratio of growth performed by grazers derived from other sources relative to that derived from both other sources and from consuming *Prochlorococcus*:

$$d_{\text{generalism}} = \frac{\gamma}{\epsilon \frac{N_P}{N_G} \psi (S+I) + \gamma} \tag{S20}$$

S2.1.2 Model inferred mortality

Total *Prochlorococcus* loss rates are defined as:

$$m_{total} = m_{\text{lysis}} + m_{\text{grazing}} + m_{\text{other}} \tag{S21}$$

where:

$$\begin{aligned} m_{\text{lysis}} &= \eta I \\ m_{\text{grazing}} &= \psi(S+I)G \\ m_{\text{other}} &= m_P (S+I)^2 \end{aligned} \tag{S22}$$

Event		Variable	Units
S and I	Average division rate	μ_{ave}	d^{-1}
	Amplitude division rate	δ_μ	unitless
	Phase of the division rate	δ_t	d
	Higher order loss rate	m_P	$L(cell \cdot d)^{-1}$
V	Adsorption	ϕ	$L\ (virus \cdot d)^{-1}$
	Latent period	LP	hours
	Burst size	β	viruses $cell^{-1}$
	Higher order viral losses	m_V	$L(virus \cdot d)^{-1}$
G	Clearance rate	ψ	$L(grazer \cdot d)^{-1}$
	Degree of generalism	γ	d^{-1}
	Higher order grazer losses	m_G	$L(grazer \cdot d)^{-1}$

Table S1: Parameters of the the ECLIP model

We defined the proportion of each mortality processes as follows:

$$\begin{aligned} r_{\text{lysis}} &= \text{mean}\left(\frac{m_{lysis}}{m_{total}}\right) \\ r_{\text{grazing}} &= \text{mean}\left(\frac{m_{grazing}}{m_{total}}\right) \\ r_{\text{other}} &= \text{mean}\left(\frac{m_{other}}{m_{total}}\right) \end{aligned} \tag{S23}$$

S2.2 Model-data integration

S2.2.1 General parameter inference implementation

We determined the parameter sets for the ECLIP model that optimized the fit of the model dynamics to field measurements by using Markov Chain Monte Carlo (MCMC) implemented in the probabilistic inference package Turing [23] in the Julia language [24]. MCMC is a class of Bayesian inference algorithms that aims to infer the probability distribution of the model parameters given the model equations, environmental data and prior beliefs [25]. We used the No-U-Turn Sampler (NUTS) implemented in Turing to sample the posterior distributions [26]. Classic Hamiltonian Monte Carlo (HMC) algorithms are sensitive to the number of steps of the simulation reducing the performance of the algorithm in high-dimension problems. NUTS is a performant alternative algorithm for MCMC that eliminates the need to set the number of steps, allowing better performance for high-dimensional parameter space and non-linear dynamical models [26].

We implemented the parameter estimation in two steps. First, we estimated the three parameter posterior distributions (μ_{ave}, δ_μ and δ_t) for the division rate function (see equation S19) using a model-inferred *Prochlorococcus* division rate estimated for the same oceanographic campaign by [27]. In a second step, we used the division parameter posteriors as priors for another parameter inference to estimate the whole set of model parameters (μ_{ave}, δ_μ, δ_t, m_P, m_V, m_G, ϕ, β, LP, and ψ) and the abundance measurements for total and infected *Prochlorococcus* cells, cyanophages and heterotrophic grazers. We repeated this second step six times by fixing the generalism term at $\gamma = 0$, 0.01, 0.05, 0.1, 0.2 and 0.5 respectively, to account to different levels of non-*Prochlorococcus* contributions to grazing.

For each implementation, we ran 4 MCMC chains for 4000 iterations with a 2000 iteration warm-up period (total iterations = 6000) and a target acceptance ratio of 0.65, allowing the algorithm to reach a stationary state. For the model $\gamma = 0.5$, we obtained chains with high autocorrelation. To decrease the autocorrelation we ran 16 independent chains of 4000 iterations and combined them in four longer chains of 16000 iterations. We then thinned these longer chains [28] by sampling every 4 iterations to obtain 4 MCMC chains of 4000 iterations with lower autocorrelation.

S2.2.2 Chain convergence analysis

To assess the convergence of the MCMC chains, we computed different indicators for each implementation [29]. For each parameter, the inter-variability of the chains was computed as the $\widehat{R}$. When the set of chains converged to the same posterior distribution, $\widehat{R}$ should be centered around 1 (with upper bound of $\widehat{R} = 1.1$), suggesting good convergence (Figure S5). We computed the ratio of effective sample size (N_{eff}) to the total iteration size ($N = 4000$) to search for potential sampling issues. Low ratio $\left(\frac{N_{eff}}{N} < 0.1\right)$, indicates potential sampling problems with higher chain auto-correlation, suggesting divergence (Figure S5). Additionally, we also computed auto-correlation for each parameter chains of the ECLIP model (Figure S8).

S2.2.3 Division function parameter inference

We fitted our division function (eq. S19) to the timeseries of division rates estimated by integrating *in situ* flow cytometry measurements with the pmb size-structured *Prochlorococcus* model described in Mattern et al. [27]. Daily division rates were estimated using a size-structured matrix population model that mechanistically describes changes in microbial cell size distribution over the day-night cycle [27]. In brief, the model assumes that changes of the cell size distribution is driven by three interconnected biological processes: carbon fixation via photosynthesis, carbon loss via respiration and exudation and cell division. We select the pmb model with a power-law size dependence on carbon fixation since there is strong evidence of an allometric growth rate in natural populations of *Prochlorococcus* [30]. The model was fit to a logarithmically spaced discrete cell size distribution of *Prochlorococcus* provided by SeaFlow, using the same priors of model parameters used in Mattern et al. [27].

This implementation helped us to refine the division priors for the whole model parameter estimation step. We used wide uniform priors for the three parameters of the division function: μ_{ave}, δ_μ and δ_t (Figure S2, Table S2). The 4 chains converged ($\widehat{R} \approx 1$, with no auto-correlation), to narrower distributions centered around $\mu_{ave} = 0.48\ d^{-1}$, $\delta_\mu = 0.75\ d^{-1}$ and $\delta_t = 0.83\ d$. Our division function predicted well the division rates from [27] (Figure S3).

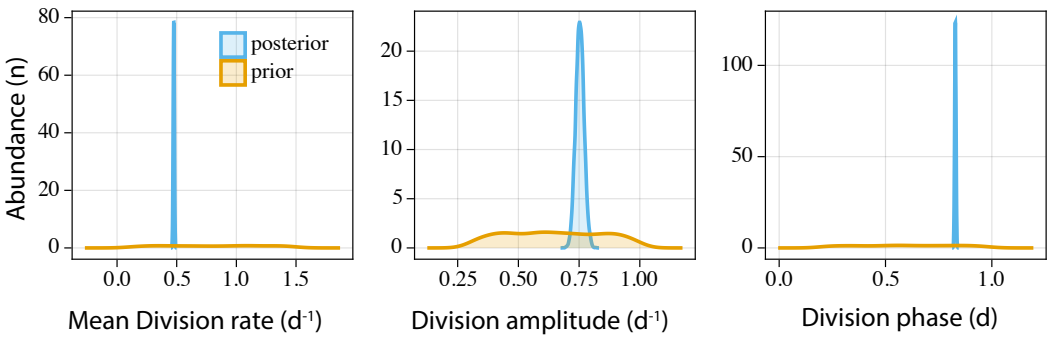

Figure S2: Priors and posteriors distribution for the division function parameters. We used wide uniform priors (orange) allowing to search a wide space for each parameter. Posteriors (blue) had narrower distributions that helped us to reduce the parameter range for the whole parameter inference step.

S2.2.4 ECLIP parameters inference implementation

To estimate the whole parameter set for the ECLIP model, we used environmental abundance data from the SCOPE HOE-Legacy 2A cruise (see Empirical data section, 2.3 in the main text, for more information). Specifically, we used total and infected *Prochlorococcus* cells, free cyanophage and heterotrophic bacteria. We inferred parameters of the ECLIP model for six levels of generalism: $\gamma = 0$, 0.01, 0.05, 0.1, 0.2, and 0.5 day^{-1}. For each implementation, we used the same priors for model parameters and log-likelihood (see next section for more information on the priors). Comparison between posteriors of the 6 models and the priors is shown in Figure S4.

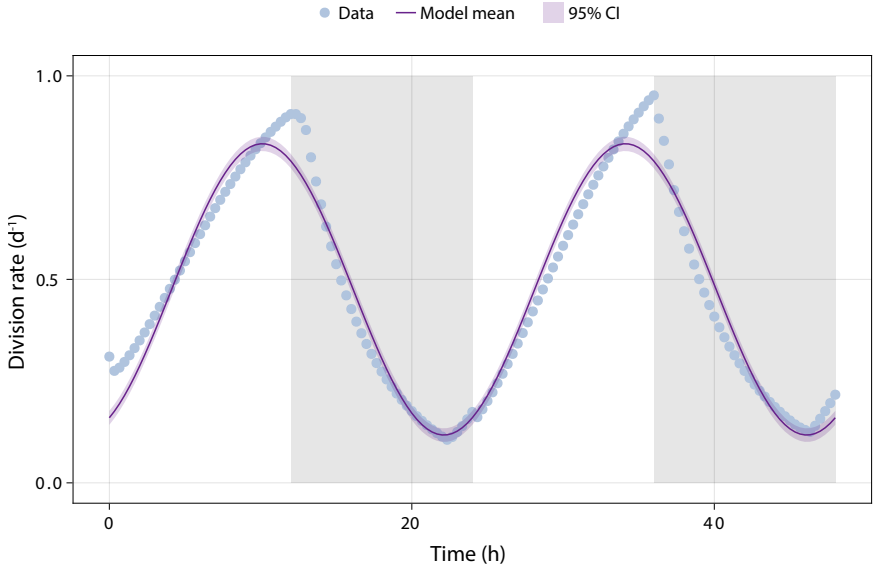

Figure S3: Division function fits. Our periodic function (purple) well represented the estimated division rate (blue dot) from [27]. Gray vertical shaded areas represent the night periods.

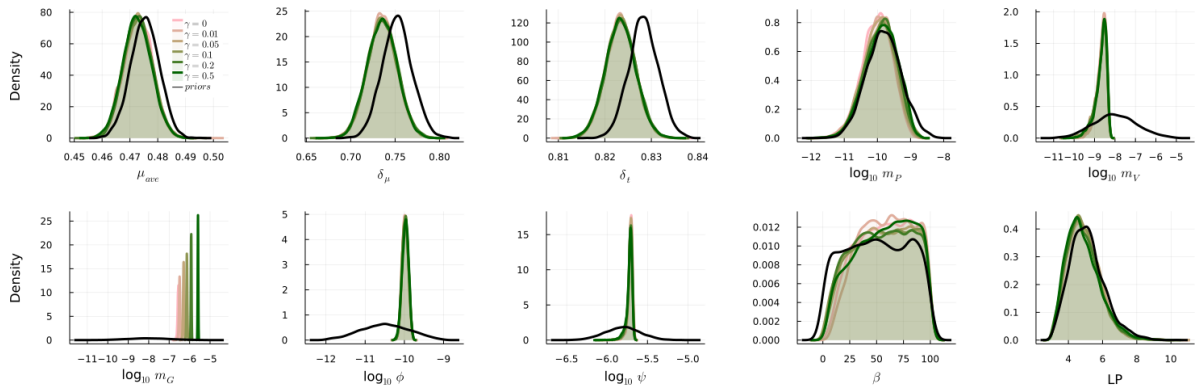

Figure S4: Comparison of parameter prior and posterior estimates in ECLIP. Prior distributions are represented in solid black lines, while posteriors are represented in colored solid lines (from pink $\gamma = 0$ d^{-1} to dark green $\gamma = 0.5$ d^{-1}).

S2.2.5 Priors and parameter ranges

We defined priors for both inference implementations, for each of the model parameters and the standard deviation σ of the likelihoods (Table S2). The ECLIP model is prone to identifiability problems due to parameter correlations, possibly leading to performance and convergence issue of the MCMC algorithm. Therefore, we weighted higher probability space for some parameters by setting Normal or log-Normal priors instead of Uniform priors for the majority of the parameters, while setting wide variance for each prior, to explore the larger parameter space as possible given ecological realistic ranges. Additionally, for the whole implementation, we fixed three parameters to reduce parameter identifiability issues: the gross growth efficiency ($\epsilon = 0.3$, [31]), and the fraction of Nitrogen content for *Prochlorococcus* ($N_P = 5.01 \times 10^{-9} \mu$g N cell^{-1}) and grazers ($N_G = 6.53 \times 10^{-6} \mu$g N cell^{-1}).

References

1. Talmy, D. *et al.* Contrasting controls on microzooplankton grazing and viral infection of microbial prey. *Frontiers in Marine Science* **6,** 182 (2019).

Implementation	Variable	Bounds	Priors
Division function	μ_{ave}	0.1 – 1.5	Uniform
	δ_μ	0 – 1	Uniform
	δ_t	0 – 1	Uniform
	$\sigma_{likelihood,div.}$	$\mathbb{R}^+$	InverseGamma(3,2)
Whole model	μ_{ave}	0.45 – 0.6	Normal$(0.475, 0.005)$
	δ_μ	0.3 – 1	Normal$(0.753, 0.017)$
	δ_t	0.2 – 1	Normal$(0.828, 0.003)$
	m_P	10^{-12} – 10^{-8}	LogNormal$\left(log\left(1.56 \times 10^{-10}\right), 1.249\right)$
	ϕ	10^{-12} – 10^{-9}	LogNormal$\left(log\left(3.2 \times 10^{-11}\right), 1.48\right)$
	LP	3 – 12	LogNormal$(log\,(5), 0.2)$
	β	0 – 100	Uniform
	m_V	10^{-11} – 10^{-5}	LogNormal$\left(log\left(1.01 \times 10^{-8}\right), 2.45\right)$
	ψ	10^{-10} – 10^{-4}	LogNormal$\left(log\left(1.55 \times 10^{-6}\right), 0.5\right)$
	m_G	10^{-11} – 10^{-5}	LogNormal$\left(log\left(1 \times 10^{-6}\right), 0.776\right)$
	$\sigma_{loglikelihood,P}$	$\mathbb{R}^+$	InverseGamma(6,1)
	$\sigma_{loglikelihood,I}$	$\mathbb{R}^+$	InverseGamma(6,1)
	$\sigma_{loglikelihood,V}$	$\mathbb{R}^+$	InverseGamma(6,1)
	$\sigma_{loglikelihood,G}$	$\mathbb{R}^+$	InverseGamma(6,1)

Table S2: Priors and parameter ranges explored for the parameter inferences

2. Berg, H. C. & Purcell, E. M. Physics of chemoreception. *Biophysical Journal* **20,** 193–219 (1977).
3. Murray, A. G. & Jackson, G. A. Viral dynamics: a model of the effects of size, shape, motion and abundance of single-celled planktonic organisms and other particles. *Marine Ecology Progress Series,* 103–116 (1992).
4. Von Smoluchowski, M. Investigation of a mathematical theory on the coagulation of colloidal suspensions. *Z. Physik. Chem.(Ger.)* **92,** 155 (1917).
5. Murata, K. *et al.* Visualizing adsorption of cyanophage P-SSP7 onto marine *Prochlorococcus*. *Scientific Reports* **7,** 44176 (2017).
6. Einstein, A. Über die von der molekularkinetischen Theorie der Wärme geforderte Bewegung von in ruhenden Flüssigkeiten suspendierten Teilchen. *Annalen der physik* **322,** 549–560 (1905).
7. Karl, D. M. & Church, M. J. Microbial oceanography and the Hawaii Ocean Time-series programme. *Nature Reviews Microbiology* **12,** 699–713 (2014).
8. Biller, S. J., Berube, P. M., Lindell, D. & Chisholm, S. W. *Prochlorococcus*: the structure and function of collective diversity. *Nature Reviews Microbiology* **13,** 13 (2015).
9. Zehr, J. P., Weitz, J. S. & Joint, I. How microbes survive in the open ocean. *Science* **357,** 646–647 (2017).
10. Kiørboe, T. How zooplankton feed: mechanisms, traits and trade-offs. *Biological Reviews* **86,** 311–339 (2011).
11. Kiørboe, T. *A mechanistic approach to plankton ecology* (Princeton University Press, 2008).
12. Ribalet, F. *et al.* SeaFlow data v1, high-resolution abundance, size and biomass of small phytoplankton in the North Pacific. *Scientific Data* **6,** 1–8 (2019).
13. Menden-Deuer, S. & Lessard, E. J. Carbon to volume relationships for dinoflagellates, diatoms, and other protist plankton. *Limnology and Oceanography* **45,** 569–579 (2000).
14. Mruwat, N. *et al.* A single-cell polony method reveals low levels of infected *Prochlorococcus* in oligotrophic waters despite high cyanophage abundances. *The ISME Journal* **15,** 41–54 (2021).
15. Connell, P. E., Ribalet, F., Armbrust, E. V., White, A. E. & Caron, D. A. Diel oscillations in feeding strategies of heterotrophic and mixotrophic nanoplankton in the North Pacific Subtropical Gyre. *Aquatic Microbial Ecology* **85,** 167–181 (2020).

16. Verity, P. G., Stoecker, D. K., Sieracki, M. E. & Nelson, J. R. Grazing, growth and mortality of microzooplankton during the 1989 North Atlantic spring bloom at 47 N, 18 W. *Deep Sea Research Part I: Oceanographic Research Papers* **40,** 1793–1814 (1993).

17. Neuer, S. & Cowles, T. J. Protist herbivory in the Oregon upwelling system. *Marine ecology progress series.* **113,** 147–162 (1994).

18. Karayanni, H., Christaki, U., Van Wambeke, F., Thyssen, M. & Denis, M. Heterotrophic nanoflagellate and ciliate bacterivorous activity and growth in the northeast Atlantic Ocean: a seasonal mesoscale study. *Aquatic Microbial Ecology* **51,** 169–181 (2008).

19. Ribalet, F. *et al.* Light-driven synchrony of *Prochlorococcus* growth and mortality in the subtropical Pacific gyre. *Proceedings of the National Academy of Sciences* **112,** 8008–8012 (2015).

20. Binder, B. J. & DuRand, M. D. Diel cycles in surface waters of the equatorial Pacific. *Deep Sea Research Part II: Topical Studies in Oceanography* **49,** 2601–2617 (2002).

21. Berube, P. M., Rasmussen, A., Braakman, R., Stepanauskas, R. & Chisholm, S. W. Emergence of trait variability through the lens of nitrogen assimilation in *Prochlorococcus. Elife* **8,** e41043 (2019).

22. Talmy, D. *et al.* An empirical model of carbon transfer to marine viruses and zooplankton grazers. *Environmental Microbiology* **21,** 2171–2181 (2019).

23. Ge, H., Xu, K. & Ghahramani, Z. *Turing: a language for flexible probabilistic inference* in *International Conference on Artificial Intelligence and Statistics, AISTATS 2018, 9-11 April 2018, Playa Blanca, Lanzarote, Canary Islands, Spain* (2018), 1682–1690. http://proceedings.mlr.press/v84/ge18b.html.

24. Bezanson, J., Edelman, A., Karpinski, S. & Shah, V. B. Julia: A fresh approach to numerical computing. *SIAM review* **59,** 65–98. https://doi.org/10.1137/141000671 (2017).

25. Lambert, B. *A students guide to Bayesian statistics* (Sage, 2018).

26. Hoffman, M. D., Gelman, A., *et al.* The No-U-Turn sampler: adaptively setting path lengths in Hamiltonian Monte Carlo. *J. Mach. Learn. Res.* **15,** 1593–1623 (2014).

27. Mattern, J. P. *et al.* A Bayesian approach to modeling phytoplankton population dynamics from size distribution time series. *PLoS Computational Biology* **18,** e1009733 (2022).

28. Link, W. A. & Eaton, M. J. On thinning of chains in MCMC. *Methods in ecology and evolution* **3,** 112–115 (2012).

29. Gelman, A., Carlin, J. B., Stern, H. S. & Rubin, D. B. *Bayesian data analysis* (Chapman and Hall/CRC, 1995).

30. Casey, J. R., Björkman, K. M., Ferrón, S. & Karl, D. M. Size dependence of metabolism within marine picoplankton populations. *Limnology and Oceanography* **64,** 1819–1827 (2019).

31. Straile, D. Gross growth efficiencies of protozoan and metazoan zooplankton and their dependence on food concentration, predator-prey weight ratio, and taxonomic group. *Limnology and Oceanography* **42,** 1375–1385 (1997).

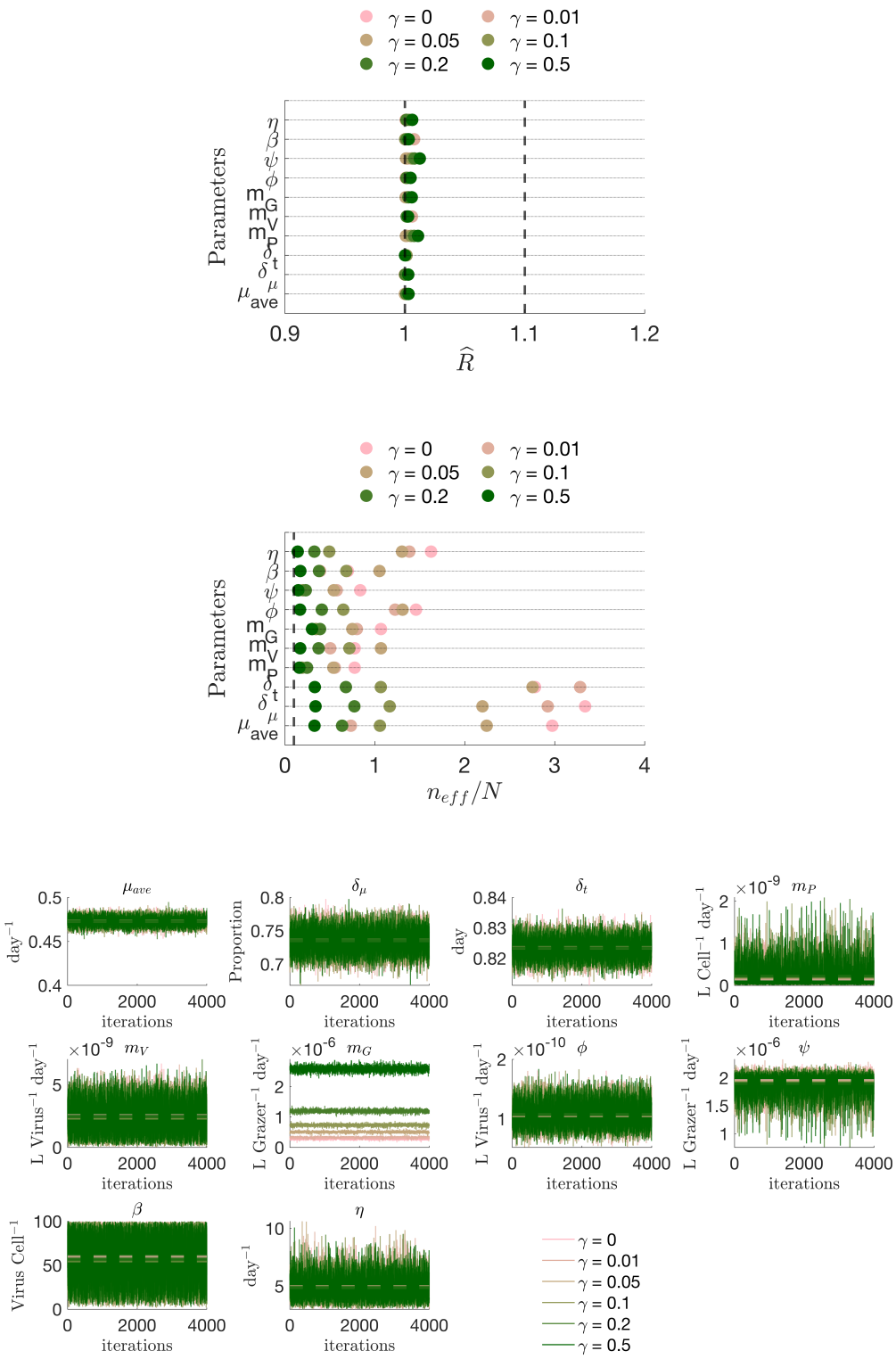

Figure S5: Assessing MCMC convergence and efficiency for ECLIP models. (a) $\widehat{R}$ convergence diagnostics. (b) Ratio of effective sample size to sample size. (c) Visualizing MCMC parameter chains for each of the ECLIP models (note density plots from chains are shown in Figure 4c). Full details of parameter bounds are shown in Table S1.

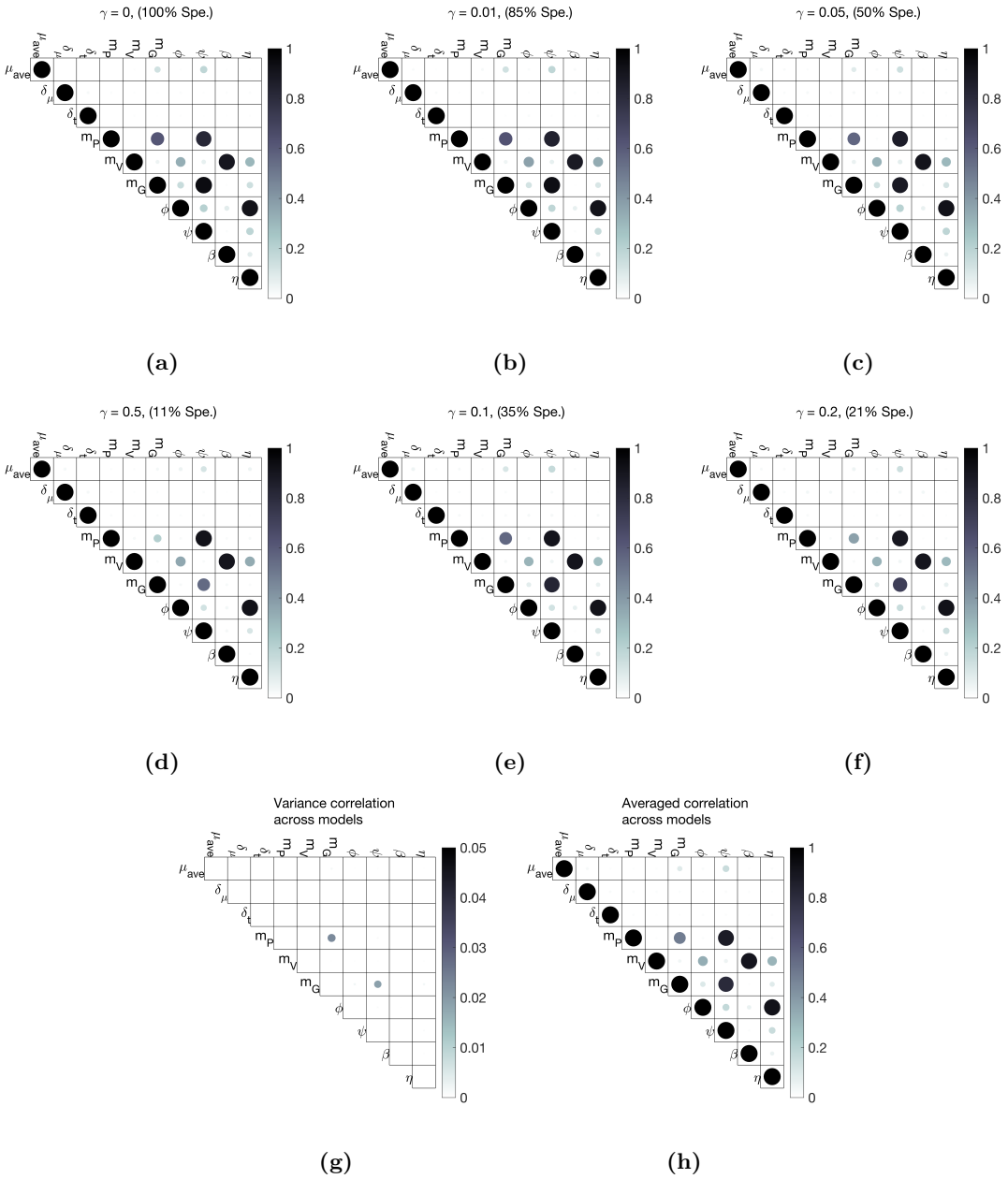

Figure S6: Identified parameter correlation in ECLIP models. Pearson correlation between parameters in MCMC chains for models with: (a) $\gamma = 0$ d^{-1}, (b) $\gamma = 0.01$ d^{-1}, (c) $\gamma = 0.05$ d^{-1}, (d) $\gamma = 0.1$ d^{-1}, (e) $\gamma = 0.2$ d^{-1}, (f) $\gamma = 0.5$ d^{-1}. (g) Pearson correlation between parameters across all MCMC chains together. (h) Average of the assessed correlations between parameters across grazer strategy models (a-f).

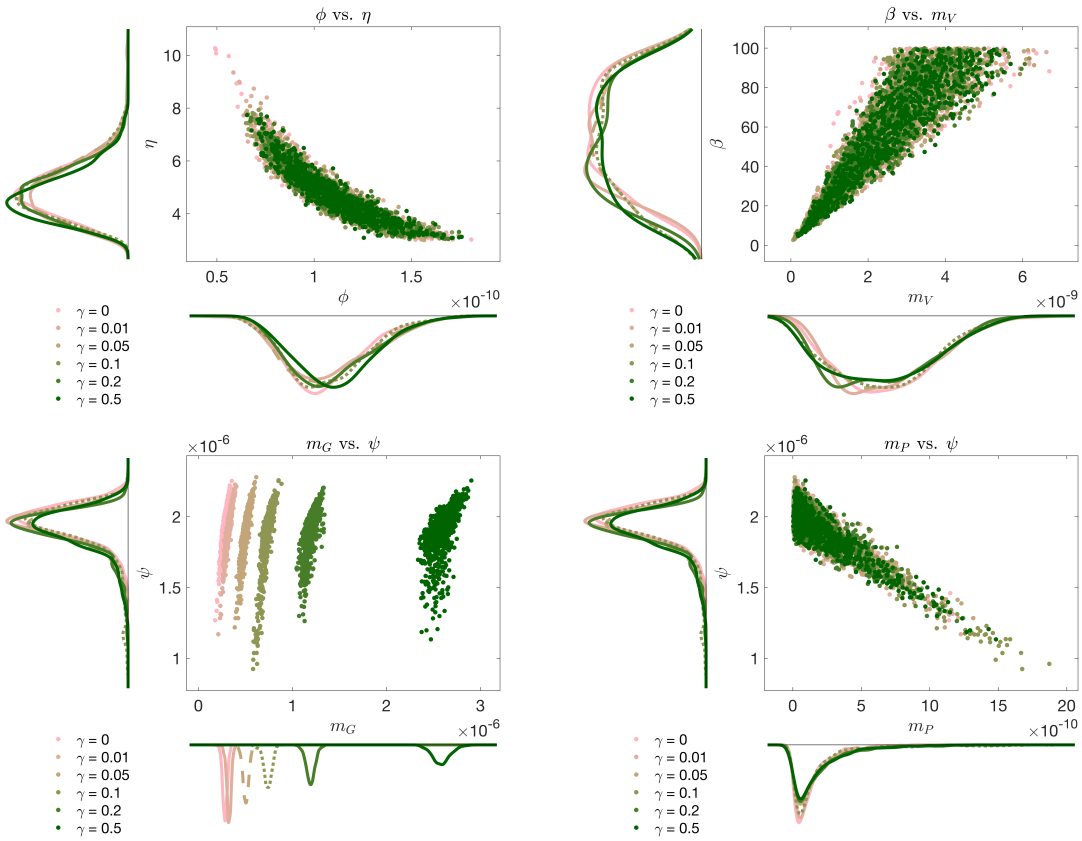

Figure S7: Examples of parameter covariance in ECLIP. Scatterplots of highly correlated ecological parameters: (a) adsorption rate (ϕ) vs lysis rate (η), (b) burst size (β) vs. viral higher order loss (m_V), (c) grazer higher order loss (m_G) vs. grazing rate (ψ), (d) *Prochlorococcus* higher order loss (m_P) vs. grazing rate (ψ).

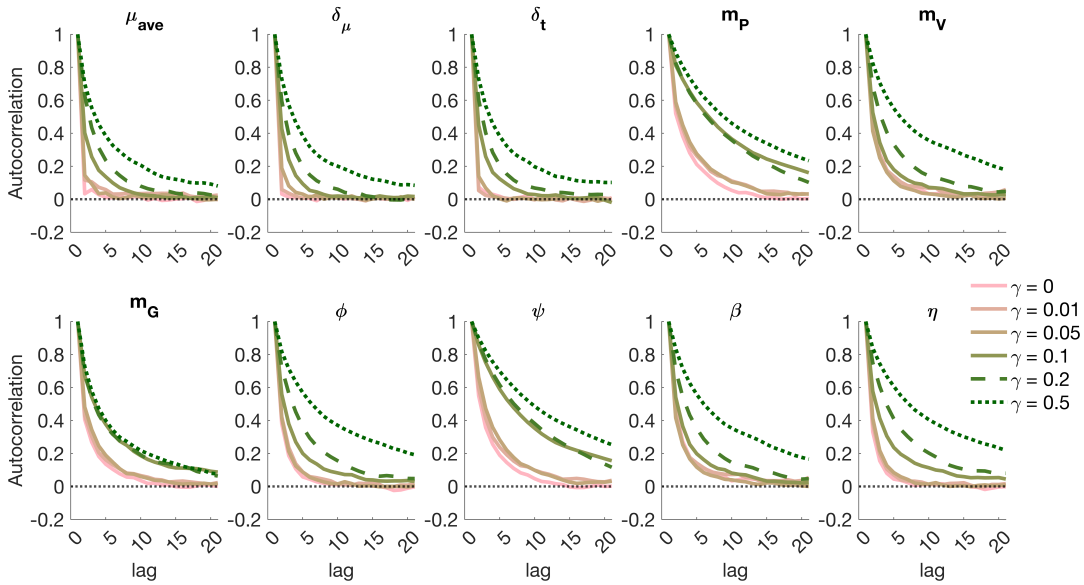

Figure S8: Parameter autocorrelation across ECLIP models. Autocorrelation was calculated as the cross-correlation of the chain with itself. Strong autocorrelation is leading to patterns or periodicity in the chain and suggest bad convergence. Our 6 models have relatively low autocorrelation for each parameter suggesting convergence.

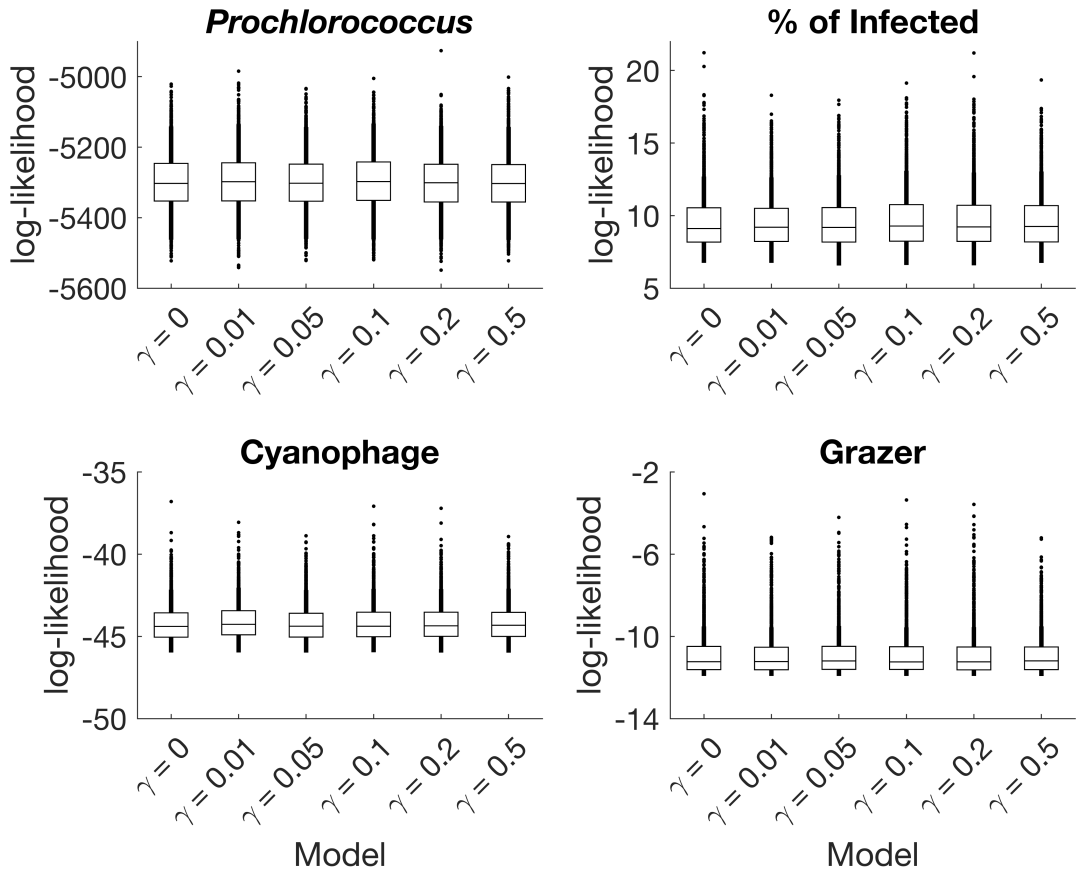

Figure S9: Negative log-likelihood for *Prochlorococcus*, % of infected *Prochlorococcus*, cyanophage and grazer across the 6 models. The negative log-likelihood function was calculated, for each chain step, as $LL(x_i) = \sum_i^n -log(p(x_i))$, where $p(x_i)$ is the model probability density function following a log-normal distribution and n the number of observations. The best model has the minimum LL. LL can only be compared between models for the same observations channels (*Prochlorococcus*, % of infected, Cyanophage or Grazer) and not between channels. The 6 models have the same ability to reproduce the observations for each chanels. Boxplots show the variability of the LL across the MCMC chain.

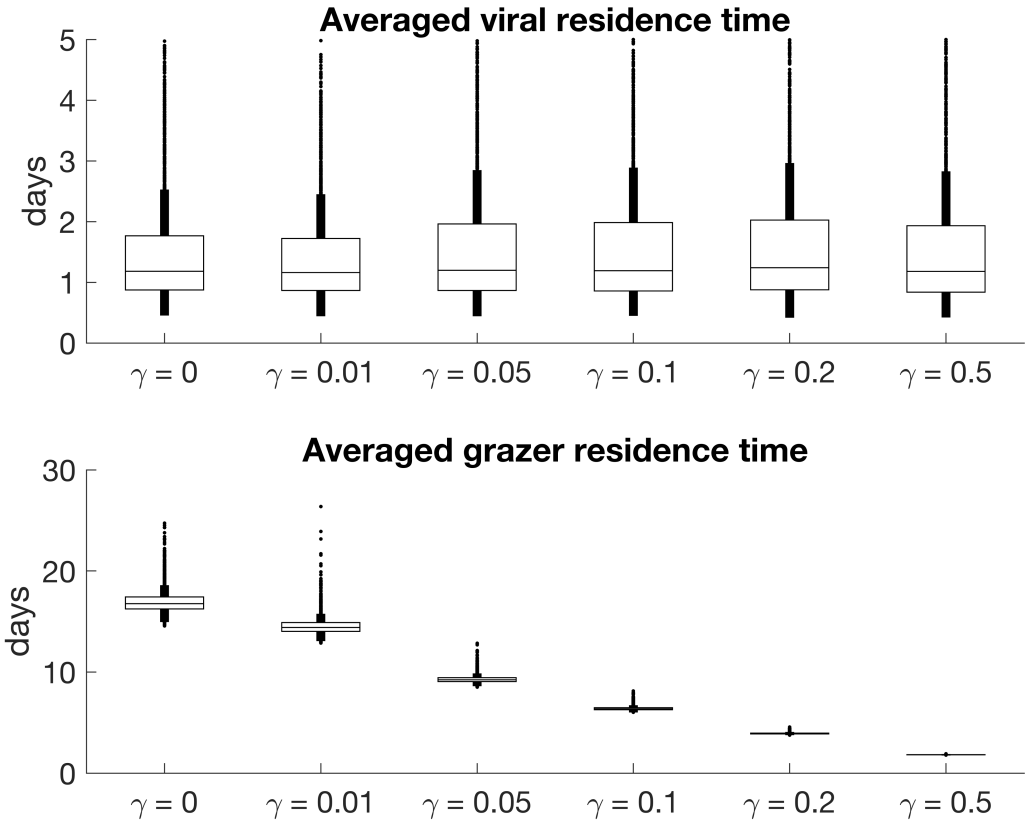

Figure S10: Averaged residence time of cyanophage (upper panel) and grazer (lower panel). Viral and grazer residence times were calculated, for each chain step, as $T_V = mean(1/(m_V \cdot V(t))$ and $T_G = mean(1/(m_G \cdot G(t))$ respectively. Median virus residence times are similar across the 6 models and range from 1.16 to 1.22 days, whereas median grazer residence times decreased from model 16.8 days (model $= 0$) to 1.8 days (model $= 0.5$). Boxplots show the variability of the log-likelihood across the MCMC chain.